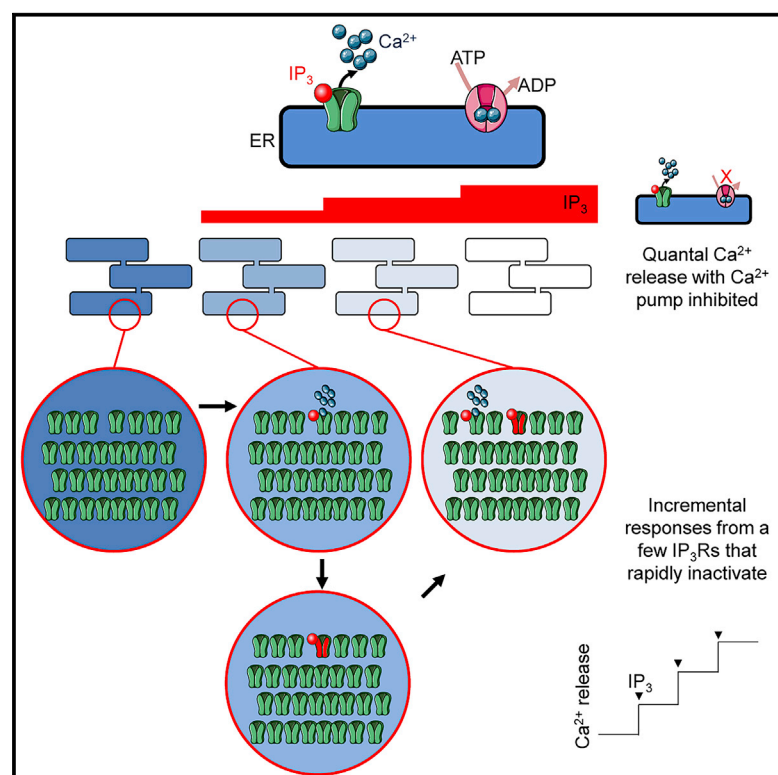


# Cell Reports

## Quantal $\text{Ca}^{2+}$ release mediated by very few $\text{IP}_3$ receptors that rapidly inactivate allows graded responses to $\text{IP}_3$

### Graphical abstract



### Authors

Ana M. Rossi, Andrew M. Riley, Geneviève Dupont, Taufiq Rahman, Barry V.L. Potter, Colin W. Taylor

### Correspondence

amr50@cam.ac.uk (A.M.R.),  
cwt1000@cam.ac.uk (C.W.T.)

### In brief

Rossi et al. define mechanisms for  $\text{IP}_3$ -evoked quantal  $\text{Ca}^{2+}$  release that reconcile response termination with undiminished sensitivity to further  $\text{IP}_3$  additions. They show that responses require very few  $\text{IP}_3$  receptors that rapidly open and then inactivate, allowing graded responses despite the ability of  $\text{IP}_3$  receptors to propagate regenerative  $\text{Ca}^{2+}$  signals.

### Highlights

- $\text{IP}_3$  evokes quantal  $\text{Ca}^{2+}$  release from the endoplasmic reticulum
- $\text{IP}_3$  receptors rapidly activate and then inactivate
- Submaximal responses to  $\text{IP}_3$  require activation of very few  $\text{IP}_3$  receptors
- Rapid activation and inactivation of very few  $\text{IP}_3$ Rs allow incremental responses to  $\text{IP}_3$



## Article

# Quantal $\text{Ca}^{2+}$ release mediated by very few $\text{IP}_3$ receptors that rapidly inactivate allows graded responses to $\text{IP}_3$

Ana M. Rossi,<sup>1,\*</sup> Andrew M. Riley,<sup>2</sup> Geneviève Dupont,<sup>3</sup> Taufiq Rahman,<sup>1</sup> Barry V.L. Potter,<sup>2</sup> and Colin W. Taylor<sup>1,4,\*</sup>

<sup>1</sup>Department of Pharmacology, University of Cambridge, Tennis Court Road, Cambridge CB2 1PD, UK

<sup>2</sup>Drug Discovery and Medicinal Chemistry, Department of Pharmacology, University of Oxford, Mansfield Road, Oxford OX1 3QT, UK

<sup>3</sup>Unité de Chronobiologie Théorique, Faculté des Sciences, CP231 Université Libre de Bruxelles (ULB), Boulevard du Triomphe, 1050 Brussels, Belgium

<sup>4</sup>Lead contact

\*Correspondence: [amr50@cam.ac.uk](mailto:amr50@cam.ac.uk) (A.M.R.), [cwt1000@cam.ac.uk](mailto:cwt1000@cam.ac.uk) (C.W.T.)

<https://doi.org/10.1016/j.celrep.2021.109932>

## SUMMARY

Inositol 1,4,5-trisphosphate receptors ( $\text{IP}_3\text{Rs}$ ) are intracellular  $\text{Ca}^{2+}$  channels that link extracellular stimuli to  $\text{Ca}^{2+}$  signals.  $\text{Ca}^{2+}$  release from intracellular stores is “quantal”: low  $\text{IP}_3$  concentrations rapidly release a fraction of the stores.  $\text{Ca}^{2+}$  release then slows or terminates without compromising responses to further  $\text{IP}_3$  additions. The mechanisms are unresolved. Here, we synthesize a high-affinity partial agonist of  $\text{IP}_3\text{Rs}$  and use it to demonstrate that quantal responses do not require heterogeneous  $\text{Ca}^{2+}$  stores.  $\text{IP}_3\text{Rs}$  respond incrementally to  $\text{IP}_3$  and close after the initial response to low  $\text{IP}_3$  concentrations. Comparing functional responses with  $\text{IP}_3$  binding shows that only a tiny fraction of a cell’s  $\text{IP}_3\text{Rs}$  mediate incremental  $\text{Ca}^{2+}$  release; inactivation does not therefore affect most  $\text{IP}_3\text{Rs}$ . We conclude, and test by simulations, that  $\text{Ca}^{2+}$  signals evoked by  $\text{IP}_3$  pulses arise from rapid activation and then inactivation of very few  $\text{IP}_3\text{Rs}$ . This allows  $\text{IP}_3\text{Rs}$  to behave as increment detectors mediating graded  $\text{Ca}^{2+}$  release.

## INTRODUCTION

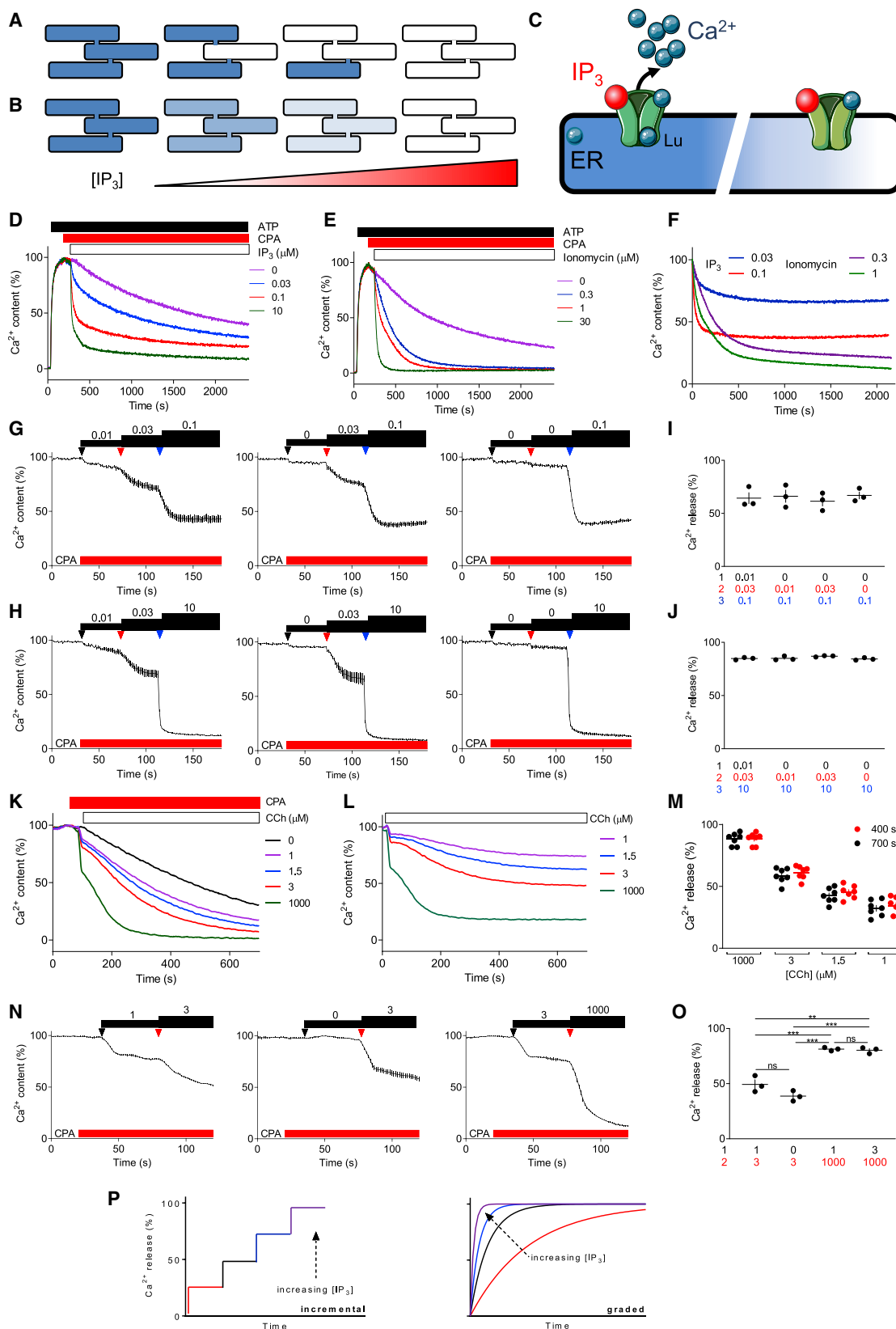
Inositol 1,4,5-trisphosphate ( $\text{IP}_3$ ) links receptors in the plasma membrane to  $\text{Ca}^{2+}$  release from the endoplasmic reticulum (ER) through  $\text{IP}_3$  receptors ( $\text{IP}_3\text{Rs}$ ), which are intracellular  $\text{Ca}^{2+}$  channels (Berridge, 2016). This redistribution of  $\text{Ca}^{2+}$  from the ER generates cytosolic  $\text{Ca}^{2+}$  signals, transfers  $\text{Ca}^{2+}$  to other organelles, and stimulates store-operated  $\text{Ca}^{2+}$  entry.  $\text{IP}_3$ -evoked  $\text{Ca}^{2+}$  signals initiate at small clusters of  $\text{IP}_3\text{Rs}$ , where  $\text{IP}_3$  binding primes  $\text{IP}_3\text{Rs}$  to open in response to  $\text{Ca}^{2+}$  released by their neighbors (Smith and Parker, 2009; Thillaiappan et al., 2017, 2021). Similar  $\text{Ca}^{2+}$ -induced  $\text{Ca}^{2+}$  release (CICR) occurs with ryanodine receptors (RyRs), the other major family of ER  $\text{Ca}^{2+}$  channels (Ríos, 2018). However, CICR is potentially explosive and might prevent cells from generating graded responses. Dispersed clusters of channels constrain regenerative propagation of  $\text{Ca}^{2+}$  signals between them (Ríos, 2018), and inhibition of  $\text{IP}_3\text{Rs}$  (and RyRs) by increased cytosolic free  $\text{Ca}^{2+}$  concentration ( $[\text{Ca}^{2+}]_c$ ) may contribute to terminating  $\text{Ca}^{2+}$  release, but it may not be the only mechanism (Wiltgen et al., 2014).

$\text{IP}_3$ -evoked  $\text{Ca}^{2+}$  release is “quantal”: submaximal  $\text{IP}_3$  concentrations rapidly release only a fraction of the  $\text{Ca}^{2+}$  stores before release terminates (Muallem et al., 1989; Taylor and Potter, 1990). This pattern of response occurs without compromising responses to further incremental increases in  $\text{IP}_3$  concentration (Meyer and Stryer, 1990), indicating that it is not mediated

by a conventional form of desensitization. Quantal  $\text{Ca}^{2+}$  release by  $\text{IP}_3\text{Rs}$  has been reported by many laboratories (reviewed in Bootman [1994] and Yamashita [2006]), and it is also a feature of RyRs (Cheek et al., 1994; Wang et al., 2004). Quantal responses have been most thoroughly examined in permeabilized cells, but they have also been reported in intact cells responding to stimuli that evoke  $\text{IP}_3$  formation (Bootman et al., 1992; Muallem et al., 1989). Hence, quantal  $\text{Ca}^{2+}$  release is an essential feature of both major families of ER  $\text{Ca}^{2+}$  channels.

The mechanism of quantal  $\text{Ca}^{2+}$  release is unknown, but it is not due to  $\text{IP}_3$  metabolism or compensatory  $\text{Ca}^{2+}$  re-uptake, nor does it require ATP (Meyer and Stryer, 1990; Taylor and Potter, 1990). Two categories of mechanism have been proposed. One suggests that submaximal concentrations of  $\text{IP}_3$  completely empty the stores that are most sensitive to  $\text{IP}_3$ , and higher  $\text{IP}_3$  concentrations then recruit the less sensitive stores (Ferris et al., 1992; Hirose and Iino, 1994; Muallem et al., 1989; Oldershaw et al., 1991; Parker and Ivorra, 1990) (Figure 1A). This model requires both extremely cooperative responses to  $\text{IP}_3$  and compartmentalized  $\text{Ca}^{2+}$  stores with heterogeneous sensitivities to  $\text{IP}_3$ . The second model suggests that  $\text{IP}_3\text{R}$  activity attenuates before  $\text{Ca}^{2+}$  stores are fully depleted (Figure 1B) (Irvine, 1990; Missiaen et al., 1992; Parys et al., 1993; Tregear et al., 1991). The mechanisms that might curtail  $\text{IP}_3\text{R}$ -mediated  $\text{Ca}^{2+}$  release include  $\text{IP}_3$ -mediated inactivation (Hajnóczky and Thomas, 1994), inhibition by increased  $[\text{Ca}^{2+}]_c$ , loss of the electrochemical  $\text{Ca}^{2+}$  gradient for  $\text{Ca}^{2+}$  release as  $\text{Ca}^{2+}$





(legend on next page)

leaves the ER without compensatory charge movements (Yamashita et al., 2006), and regulation of IP<sub>3</sub>Rs by luminal Ca<sup>2+</sup> (Figure 1C). The latter mechanism proposes that opening of an IP<sub>3</sub>R requires binding of IP<sub>3</sub> and of Ca<sup>2+</sup> at both the cytosolic and luminal sides of the IP<sub>3</sub>R (Irvine, 1990; Marchant and Taylor, 1997). Regulation by luminal Ca<sup>2+</sup> predicts that as ER [Ca<sup>2+</sup>] falls, the sensitivity of IP<sub>3</sub>Rs to cytosolic IP<sub>3</sub> and Ca<sup>2+</sup> declines, and Ca<sup>2+</sup> release then terminates with Ca<sup>2+</sup> trapped in the ER (Figure 1C). In the 30 years since quantal Ca<sup>2+</sup> release was first identified (Muallem et al., 1989; Taylor and Potter, 1990), numerous studies have confirmed the phenomenon and provided evidence that supports or challenges each mechanism (Yamashita, 2006). Single-channel recordings from IP<sub>3</sub>Rs (Ionescu et al., 2006; Taufiq-Ur-Rahman et al., 2009) and high-resolution optical methods (Callamaras and Parker, 2000) have also failed to identify the mechanisms underlying incremental responses to IP<sub>3</sub>.

Here, we synthesize a high-affinity, partial agonist of IP<sub>3</sub>R with exceptionally low efficacy, and use it to establish that quantal responses are not mediated by all-or-nothing emptying of stores with heterogeneous sensitivities to IP<sub>3</sub> (Figure 1A). We show that all three subtypes of IP<sub>3</sub>Rs mediate incremental responses to IP<sub>3</sub>, and that the responses arise from a tiny fraction of a cell's IP<sub>3</sub>Rs opening in response to IP<sub>3</sub> and then inactivating. This mechanism resolves long-standing confusion and establishes how cells respond to incremental changes in IP<sub>3</sub> concentration.

## RESULTS AND DISCUSSION

### Quantal Ca<sup>2+</sup> release by all IP<sub>3</sub>R subtypes

To measure IP<sub>3</sub>-evoked Ca<sup>2+</sup> release without the opposing activity of ER Ca<sup>2+</sup> pumps (sarcoplasmic/ER Ca<sup>2+</sup>-ATPases [SERCAs]), the ER of permeabilized DT40 cells expressing only

IP<sub>3</sub>R1 (DT40-IP<sub>3</sub>R1 cells) was loaded with Mag-fluo 4, a low-affinity Ca<sup>2+</sup> indicator (Rossi and Taylor, 2020). ATP was added to fuel Ca<sup>2+</sup> uptake before addition of cyclopiazonic acid (CPA) to inhibit SERCAs; IP<sub>3</sub> was then added to stimulate Ca<sup>2+</sup> release (Figure 1D). A maximally effective IP<sub>3</sub> concentration released ~70% of the ER Ca<sup>2+</sup> content. Submaximal IP<sub>3</sub> concentrations rapidly released a smaller fraction of the stores, after which there was no further effect of IP<sub>3</sub> on the rate of Ca<sup>2+</sup> release or its effect was much reduced (Figure 1D). These quantal responses to IP<sub>3</sub> are clearest after correction for the basal Ca<sup>2+</sup> leak evident after SERCA inhibition (Figure 1F). The responses to IP<sub>3</sub> are very different to those evoked by the Ca<sup>2+</sup> ionophore, ionomycin, which stimulated monophasic Ca<sup>2+</sup> loss from the entire ER at rates that increased with ionomycin concentration (Figures 1E, 1F, S1A, and S1B). Similar quantal responses from type 1 IP<sub>3</sub>R (IP<sub>3</sub>R1) were observed with IP<sub>3</sub> in the presence of the K<sup>+</sup> ionophore, valinomycin, to dissipate any ER membrane potential; with Cs<sup>+</sup> replacing K<sup>+</sup> to inhibit K<sup>+</sup> channels; with mitochondria inhibited; with IP<sub>3</sub> added in larger volumes to avoid possible artifacts arising from bolus additions; and with inositol 2,4,5-trisphosphate ((2,4,5)IP<sub>3</sub>), a non-metabolized analog of IP<sub>3</sub> (Hill et al., 1988) (Figures S1C–S1J).

Although responses to low IP<sub>3</sub> concentrations rapidly attenuated (Figures 1D, 1F, and S1B), subsequent addition of more IP<sub>3</sub> evoked further rapid Ca<sup>2+</sup> release. Furthermore, the fraction of the Ca<sup>2+</sup> stores released by maximal or submaximal IP<sub>3</sub> concentrations was the same whether IP<sub>3</sub> was delivered immediately at its final concentration or as incremental additions (Figures 1G–1J). Similar “incremental” responses (Beecroft and Taylor, 1997; Ferris et al., 1992; Meyer and Stryer, 1990) were obtained in the presence of the fast Ca<sup>2+</sup> buffer, BAPTA, at a concentration (10 mM) sufficient to rapidly buffer even very local

### Figure 1. Quantal Ca<sup>2+</sup> release by IP<sub>3</sub>Rs

(A–C) Proposed mechanisms for quantal Ca<sup>2+</sup> release: all-or-nothing emptying of stores with different IP<sub>3</sub> sensitivities (A), or mechanisms that terminate Ca<sup>2+</sup> release before stores have fully emptied (B). The latter could be mediated by luminal Ca<sup>2+</sup> regulating IP<sub>3</sub>Rs, such that as the luminal [Ca<sup>2+</sup>] falls after IP<sub>3</sub>R activation, Ca<sup>2+</sup> dissociates from the luminal site (Lu), and IP<sub>3</sub>Rs close trapping Ca<sup>2+</sup> within the ER (C) (Irvine, 1990).

(D and E) Ca<sup>2+</sup> content of the ER of permeabilized Mag-fluo 4-loaded DT40-IP<sub>3</sub>R1 cells after addition of ATP (1.5 mM) followed by CPA (10 μM) to inhibit SERCAs, and then the indicated concentrations (μM) of IP<sub>3</sub> (D) or ionomycin (E). Results (typical of three to four experiments, each with two replicates) show Ca<sup>2+</sup> content (%) relative to steady-state Ca<sup>2+</sup> content; (D) is reproduced from Rossi and Taylor (2020).

(F) Responses to IP<sub>3</sub> and ionomycin plotted after subtraction of the basal Ca<sup>2+</sup> leak.

(G and H) Effects of submaximal (100 nM) (G) or maximal (10 μM) (H) concentrations of IP<sub>3</sub> added directly or by incremental additions to permeabilized DT40-IP<sub>3</sub>R1 cells. Results show mean ± SD of three replicates.

(I and J) Summary results (individual values, mean ± SEM, n = 3, each with three replicates) show the Ca<sup>2+</sup> released from the stores of permeabilized DT40-IP<sub>3</sub>R1 cells (determined at 150 s) for the three incremental additions (cumulative IP<sub>3</sub> concentrations shown in μM). The final Ca<sup>2+</sup> release was not significantly different between any of the incremental additions (one-way repeated ANOVA with Bonferroni's multiple comparisons test).

(K) Ca<sup>2+</sup> content of the ER of intact wild-type HEK expressing G-CEPIA1er after addition of CPA (5 μM) to inhibit SERCAs, and then the indicated concentrations of carbachol (CCh, μM). Results (typical of seven experiments, each with three replicates) show Ca<sup>2+</sup> content (%) relative to the Ca<sup>2+</sup> content determined before adding CPA.

(L) Responses to the indicated concentrations of carbachol in intact wild-type HEK expressing G-CEPIA1er after subtraction of the basal Ca<sup>2+</sup> leak.

(M) Summary results (mean ± SEM, n = 7, each with three replicates) show the Ca<sup>2+</sup> released from the stores of intact wild-type HEK expressing G-CEPIA1er determined at 400 and 700 s for the indicated concentrations of carbachol. The Ca<sup>2+</sup> release at 400 and 700 s was not significantly different at any of the carbachol concentrations (one-way repeated ANOVA with Bonferroni's multiple comparisons test).

(N) Incremental responses from intact wild-type HEK cells to the indicated concentrations of carbachol added after CPA (5 μM) and recorded using G-CEPIA1er (cumulative carbachol concentrations are shown in μM).

(O) Summary results from intact wild-type HEK cells expressing G-CEPIA1er (individual values, mean ± SEM, n = 3, each with 8–12 replicates) show Ca<sup>2+</sup> released from the stores (determined at 150 s) for the incremental additions (cumulative carbachol concentrations shown in μM). \*\*p < 0.01, \*\*\*p < 0.001; ns, not significant (for indicated comparisons; one-way repeated ANOVA with Bonferroni's multiple comparisons test).

(P) Incremental responses to IP<sub>3</sub> compared with the graded rates of Ca<sup>2+</sup> release expected if increasing concentrations of IP<sub>3</sub> uniformly increased the permeability of the ER to Ca<sup>2+</sup>.

See also Figures S1–S4.

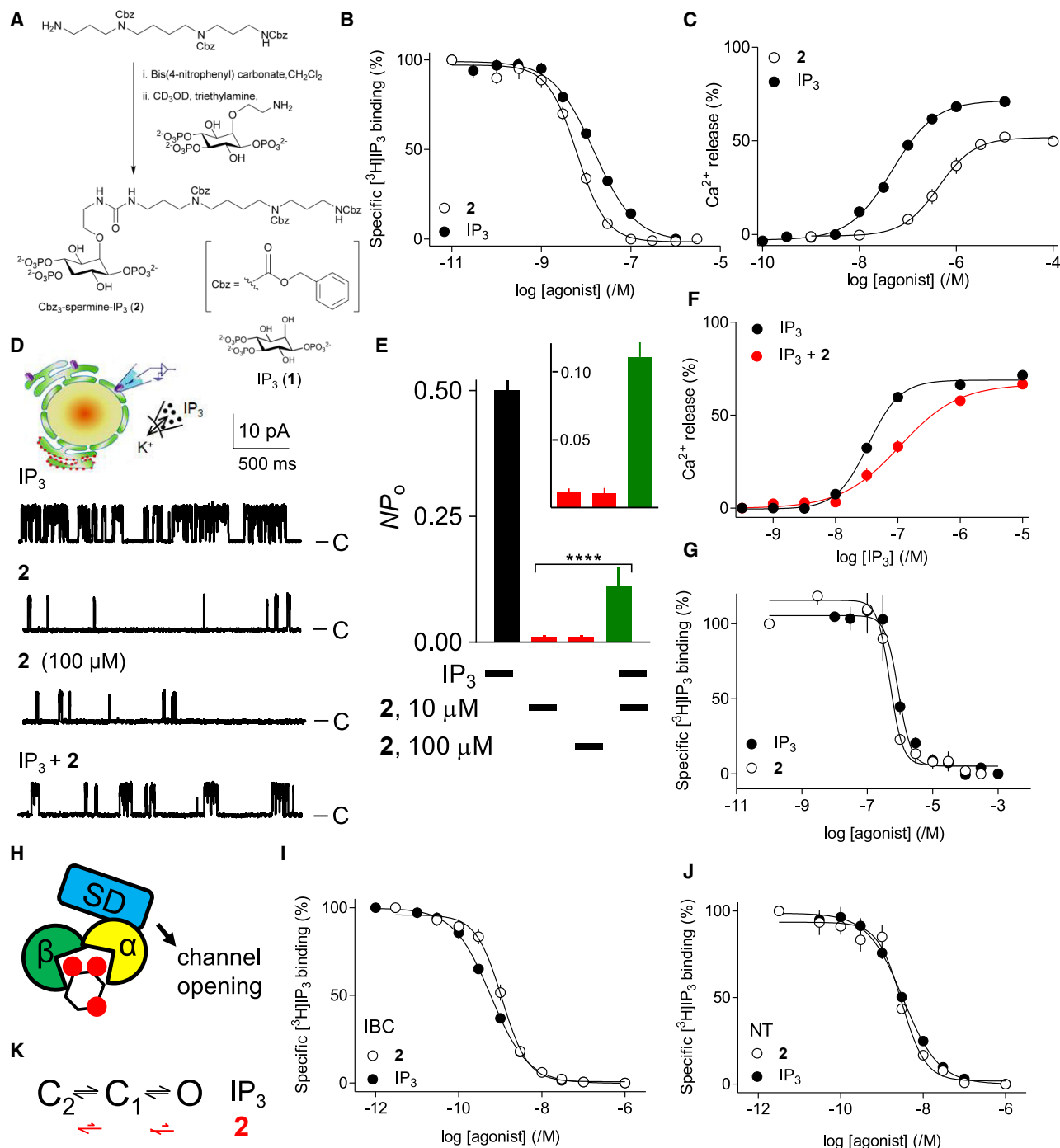


**Figure 2. A 2-O-modified analog of IP<sub>3</sub> (**2**) is a high-affinity, partial agonist**

(A) Synthetic scheme for **2** and structure of IP<sub>3</sub>.

(B) Equilibrium-competition binding to purified full-length IP<sub>3</sub>R1 using [<sup>3</sup>H]IP<sub>3</sub> (1.5 nM) and the indicated concentrations of IP<sub>3</sub> or **2** in Tris-EDTA medium (TEM) at 4°C (mean ± SEM, n = 7, many error bars are smaller than the symbols).

(C) Effects of IP<sub>3</sub> or **2** on Ca<sup>2+</sup> release (determined after 20 s) from permeabilized DT40-IP<sub>3</sub>R1 cells (mean ± SEM, n = 3, each with three replicates).

(D) Patch-clamp recordings, typical of at least five recordings, from excised nuclear patches of DT40-IP<sub>3</sub>R1 cells, at a holding potential of +40 mV with K<sup>+</sup> as the charge carrier, and ligands within the pipette (cytosolic surface; IP<sub>3</sub>, 10 μM; **2**, 10 μM, except where shown otherwise). C, closed state.

(E) Summary results (mean ± SEM, n = 5–7) show channel activity (NP<sub>o</sub>) for the indicated stimuli (enlarged in the inset). \*\*\*\*p < 0.0001, ANOVA with Bonferroni's test, relative to IP<sub>3</sub> alone.

(legend continued on next page)



increases in  $[Ca^{2+}]_c$  (Vais et al., 2012). This indicates that inhibition of  $IP_3$ R by increases in  $[Ca^{2+}]_c$  are not required for incremental responses (Figures S2A–S2F). That conclusion is consistent with two additional lines of evidence. First,  $IP_3$ R from *Capsaspora owczarzaki* are not regulated by cytosolic  $Ca^{2+}$ , but they do mediate quantal  $Ca^{2+}$  release (Alzayady et al., 2015). Second, in ER depleted of  $Ca^{2+}$ , retrograde movement of  $Mn^{2+}$  through open  $IP_3$ R can be used to report  $IP_3$ R opening. Under these conditions, responses to  $IP_3$  have been reported to be quantal, but only after fragmentation of the ER (Hajnóczky et al., 1994; Renard-Rooney et al., 1993). Responses were also incremental in permeabilized DT40 cells expressing only  $IP_3$ R2 or  $IP_3$ R3 (Figures S2G–S2J), and in wild-type human embryonic kidney (HEK) cells, which express all three  $IP_3$ R subtypes (Mataragka and Taylor, 2018) (Figure S3). In each case, the total amount of  $Ca^{2+}$  released by a submaximal concentration of  $IP_3$  was the same whether  $IP_3$  was presented as a single addition or as incremental additions. Incremental responses to  $IP_3$  were also observed using a low-affinity genetically encoded  $Ca^{2+}$  indicator targeted to the ER lumen (G-CEPIA1er) (Suzuki et al., 2014) (Figures S4A–S4H).

In single-cell analyses of permeabilized HEK cells stably expressing G-CEPIA1er, all cells responded to a maximal  $IP_3$  concentration with a rapid decrease in ER luminal  $[Ca^{2+}]$ . Submaximal  $IP_3$  concentrations rapidly released a fraction of the  $IP_3$ -sensitive stores, and the response then terminated without preventing subsequent responses to a maximal  $IP_3$  concentration (Figures S4I–S4N). Quantal responses observed in populations of permeabilized cells are not, therefore, due to all-or-nothing responses from different cells with heterogeneous  $IP_3$  sensitivities. In permeabilized hepatocytes too, quantal responses to  $IP_3$  were observed in single cells (Renard-Rooney et al., 1993). We also measured changes in G-CEPIA1er fluorescence within small subcellular regions and, although the spatial resolution was limited, the results suggest that different regions within a HEK cell have similar sensitivity to  $IP_3$  (Figures S4K–S4N).

It has been reported that quantal responses to  $IP_3$  are observed in permeabilized hepatocytes only when permeabilization is accompanied by fragmentation of the ER (Renard-Rooney et al., 1993). Most studies do not address whether the ER remains continuous after permeabilization. In our analyses of permeabilized HEK cells, there is some fragmentation of the ER, whether reported by G-CEPIA1er or compartmentalized Mag-fluo 4, and attempts to avoid it by adjusting conditions failed to achieve ATP-dependent  $Ca^{2+}$  uptake without some ER fragmentation (Figure S4O). However, several lines of evidence establish that quantal responses are not an artifact arising from ER fragmentation. First,

others have observed quantal responses from stimuli that evoke  $IP_3$  formation in intact cells (Bootman et al., 1992; Muallem et al., 1989). By measuring quantal responses directly using a  $Ca^{2+}$  indicator within the ER lumen, we confirmed that stimulation of the endogenous muscarinic acetylcholine receptors of HEK cells with carbachol to evoke  $IP_3$  formation caused quantal  $Ca^{2+}$  release from intracellular stores (Figures 1K–1M). Successive additions of carbachol evoked incremental responses (Figures 1N and 1O). Second, fragmentation of the ER might create the heterogeneous  $Ca^{2+}$  stores required for the all-or-nothing model of quantal  $Ca^{2+}$  release (Figure 1A), but it is difficult to envisage how it might create the conditions required for a model where  $IP_3$ R close before the stores have fully emptied (Figure 1B). Our subsequent experiments demonstrate that all-or-nothing emptying of discrete  $Ca^{2+}$  stores cannot explain quantal responses (see Figures 2 and 3), and we provide direct evidence that  $IP_3$ R inactivate before the stores have emptied (see Figures 5, 6, and 7).

The results so far confirm that incremental responses to  $IP_3$  occur within single cells, they are not a consequence of cell permeabilization, and they are not mediated by increases in  $[Ca^{2+}]_c$ , by  $IP_3$  metabolism, or by ineffective movement of counter-ions, nor do mitochondria contribute. Incremental responses to  $IP_3$  (Figure 1P) are a feature of all  $IP_3$ R subtypes, and genetically encoded  $IP_3$ R heterogeneity is not required for quantal  $Ca^{2+}$  release. The present results do not, however, distinguish between the proposed mechanisms (Figures 1A–1C).

### Characterization of a high-affinity, weak partial agonist of $IP_3$ R

Because partial agonists activate receptors less effectively than do full agonists (Rossi et al., 2009), we predicted that if a weak partial agonist occupied all  $IP_3$ R and evoked quantal  $Ca^{2+}$  release, the quantal mechanism could not be due to heterogeneous  $IP_3$ R sensitivity. We previously developed 2-O-modified  $IP_3$  analogs that are partial agonists (Rossi et al., 2009), but none has sufficiently low efficacy for our present needs. Reasoning that enlarging the 2-O-substituent might further reduce efficacy, we synthesized additional analogs and found Cbz<sub>3</sub>-spermine- $IP_3$  (compound 2) to be an exceptionally weak partial agonist (Figure 2A). Compound 2 bound to  $IP_3$ R1 with about 2-fold greater affinity than  $IP_3$  (Figure 2B), but it was significantly less potent than  $IP_3$  in stimulating  $Ca^{2+}$  release from permeabilized DT40- $IP_3$ R1 cells (Figures 2C; Table S1) or wild-type HEK cells (Table S2). The difference between binding and functional analyses is captured by comparing the ligand concentrations required to release 50% of the  $IP_3$ -sensitive  $Ca^{2+}$  stores ( $EC_{50}$ ) and to occupy 50% of  $IP_3$ -binding sites ( $K_D$ , equilibrium

(F) Permeabilized DT40- $IP_3$ R1 cells stimulated (30 s) with 2 (1  $\mu$ M, which evoked  $31\% \pm 7\%$   $Ca^{2+}$  release) were then stimulated with the indicated concentrations of  $IP_3$ .  $Ca^{2+}$  release evoked by  $IP_3$  (determined after a further 20 s) is shown as a percentage of the store content after the first stimulus (mean  $\pm$  SEM,  $n \geq 4$ , each with three replicates).

(G) Equilibrium-competition binding to cerebellar membranes using [ $^3$ H] $IP_3$  (7.5 nM) and the indicated concentrations of  $IP_3$  or 2 in CLM at 20°C (mean  $\pm$  SEM,  $n = 3$ –4 with duplicate determinations).  $pK_D$  values were  $6.10 \pm 0.06$  (mean  $\pm$  SEM,  $n = 4$ ,  $K_D = 794$  nM) for  $IP_3$  and  $6.26 \pm 0.01$  ( $n = 3$ ,  $K_D = 549$  nM) for 2. Hill coefficients ( $h$ ) were  $3.2 \pm 1.3$  and  $2.0 \pm 0.7$  for  $IP_3$  and 2.

(H)  $IP_3$  binds between the  $\alpha$  and  $\beta$  domains of the IBC, but the SD is required for  $IP_3$  to evoke channel opening.

(I and J) Equilibrium-competition binding of  $IP_3$  and 2 to the IBC or NT using [ $^3$ H] $IP_3$  (0.3 or 0.75 nM for IBC and NT, respectively). Mean  $\pm$  SEM,  $n = 4$ .

(K)  $IP_3$ R moves between an unknown numbers of closed states (C) to an open state (O) after  $IP_3$  binding. Rate(s) of movement through the closed to the open state occur more slowly with 2 bound to the  $IP_3$ R.

Tables S1–S3 summarize the properties of  $IP_3$  and 2.

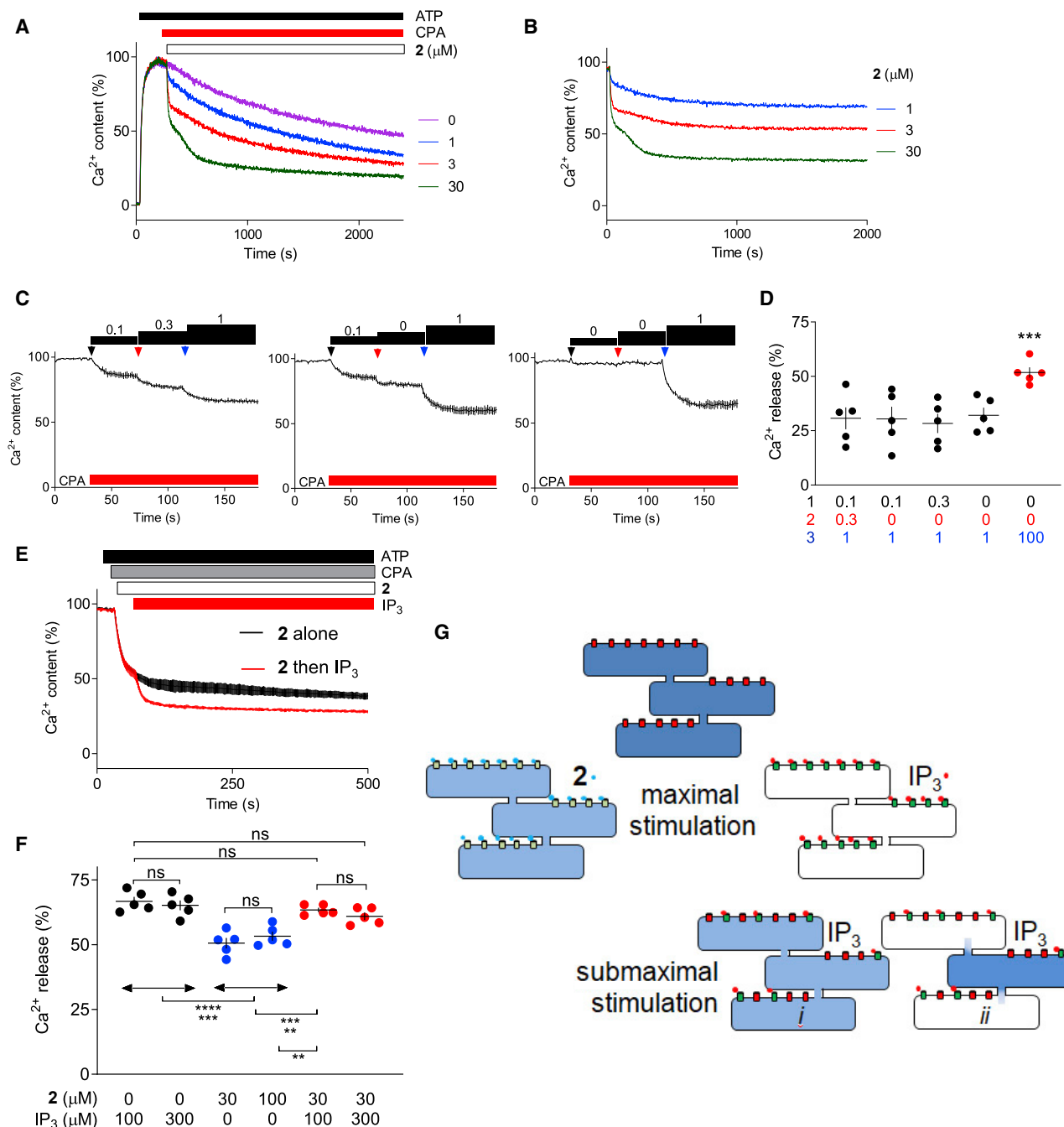


**Figure 3. Quantal responses are not mediated by heterogeneous stores**

(A) Ca<sup>2+</sup> content of the ER of populations of permeabilized DT40-IP<sub>3</sub>R1 cells after addition of ATP, CPA (10  $\mu\text{M}$ ), and then the indicated concentrations of **2**. Results are typical of three experiments, each with duplicate determinations.

(B) Responses to **2** shown after subtraction of the basal Ca<sup>2+</sup> leak.

(C) Effects of a submaximal concentration of **2** (1  $\mu\text{M}$ ) added directly or by incremental additions. Results show mean  $\pm$  SD of three replicates.

(D) Summary results (individual values, mean  $\pm$  SEM,  $n = 5$ , each with three replicates) show the final Ca<sup>2+</sup> content of the stores of permeabilized DT40-IP<sub>3</sub>R1 cells (determined at 150 s). A maximal concentration of **2** (30  $\mu\text{M}$ ) released 52%  $\pm$  3% of the Ca<sup>2+</sup> stores (red symbols). \*\*\* $p < 0.001$ , one-way repeated ANOVA with Bonferroni's test relative to all other values.

(E) Ca<sup>2+</sup> release from wild-type HEK cells evoked by **2** (30  $\mu\text{M}$ ) alone or followed by a supra-maximal concentration of IP<sub>3</sub> (100  $\mu\text{M}$ ). Mean of duplicate determinations.

(legend continued on next page)

dissociation constant); the ratio ( $EC_{50}^I/K_D$ ) is 41-fold greater for **2** than for  $IP_3$  (Table S1). The weakest known partial agonist with an affinity comparable to  $IP_3$  (compound 4 in Rossi et al., 2009) has an  $EC_{50}^I/K_D$  ratio only 5.7-fold greater than that of  $IP_3$ .

In patch-clamp recordings from the outer nuclear envelope, which is continuous with the ER, the increase in channel open probability ( $NP_o$ ) of  $IP_3R1$  was the same for 10 and 100  $\mu M$  of **2**, confirming that both concentrations were maximally effective (Figures 2D and 2E). However, the maximal  $NP_o$  for **2** was 40-fold less than for  $IP_3$ ; the single-channel conductance ( $\gamma_K$ ) was the same for both agonists (Figures 2D and 2E; Table S1). Because partial agonists bind to the same site as full agonists, but less effectively activate the receptor, they behave as competitive antagonists of full agonists. This behavior is evident in patch-clamp and  $Ca^{2+}$ -release assays, where **2** reduced the response to  $IP_3$  (Figures 2D–2F). These observations, which are expected for a partial agonist, are important for subsequent experiments because they demonstrate that  $IP_3$  and **2** compete for occupancy of the same  $IP_3Rs$ , but **2** causes less effective activation.

The  $K_D$  of **2** determined from dose-ratio analysis ( $K_D = 426$  nM) (Table S3) was similar to the half-maximally effective concentration of **2** in  $Ca^{2+}$ -release assays ( $EC_{50} = 479$  nM, Table S1), as expected for a weak partial agonist. The  $K_D$  for **2** derived from functional assays ( $\sim 450$  nM) is much greater than that determined by radioligand binding (5.2 nM) because they use different assay conditions (Ding et al., 2010). However, in binding analyses performed under conditions that mimic functional assays, the  $K_D$  for **2** was 549 nM, which is comparable to its  $EC_{50}$  for  $Ca^{2+}$  release, and 1.5-fold lower than the  $K_D$  for  $IP_3$  determined under these conditions (794 nM) (Figure 2G).

We reported previously that the reduced open probability ( $P_o$ ) of  $IP_3Rs$  activated by partial agonists was due to an increase in mean channel closed time ( $\tau_c$ ), with no effect on mean open time ( $\tau_o$ ) (Rossi et al., 2009). Similar behavior appears to underlie the reduced efficacy of **2** because the modest ( $\sim 2$ -fold) decrease in  $\tau_o$  (relative to  $IP_3$ ) is insufficient to explain the 40-fold decrease in  $NP_o$  (Table S1). With such low  $P_o$ , it is impracticable to determine  $\tau_c$  directly for **2**.

$IP_3$  binds to the  $IP_3$ -binding core of the  $IP_3R$  (IBC, residues 224–604) (Bosanac et al., 2002), but communication with the channel requires the suppressor domain (SD, residues 1–223) (Rossi et al., 2009; Yoshikawa et al., 1999) (Figure 2H). The difference in ligand affinities ( $\Delta\Delta G = \Delta G^{IBC} - \Delta G^{NT}$ , where  $\Delta G = -RT \ln K_D$ ) for the IBC and N-terminal (NT, residues 1–604) reports the binding energy diverted into changing the NT conformation (Rossi et al., 2009). Analyses of  $IP_3$  and **2** binding to the IBC and NT confirm that  $IP_3$  diverts more energy into changing the NT conformation than does **2** (Figures 2I and 2J; Table S1).

We conclude that **2** is a high-affinity, partial agonist of  $IP_3R$ . It is the weakest known partial agonist with high affinity for  $IP_3R$ . The basis of its low efficacy is similar to that of related partial agonists (Rossi et al., 2009): it perturbs communication between

the IBC and SD, causing the channel to dwell longer in a closed state and so open infrequently (Figure 2K). Our results suggest strategies to develop high-affinity antagonists of  $IP_3R$  and they provide the tool needed to assess whether all-or-nothing emptying of  $Ca^{2+}$  stores with heterogeneous  $IP_3R$  sensitivities underlies quantal responses (Figure 1A).

### Quantal responses are not mediated by heterogeneous stores

Compound **2** stimulated quantal  $Ca^{2+}$  release, and the responses to sequential additions were incremental (Figures 3A–3D). However, the quantal response evoked by a maximally effective concentration of **2** (Figures 3A and 3D) was smaller than the maximal response to  $IP_3$  (Figure 2C). Hence, even when all  $IP_3Rs$  are occupied by **2**, the  $IP_3$ -sensitive  $Ca^{2+}$  stores are not fully depleted. However, the  $Ca^{2+}$  stores remain sensitive to a subsequent  $IP_3$  addition, albeit at a high concentration of  $IP_3$  because it must now surmount the competitive antagonism of **2** (Figures 3E and 3F). Since **2** evokes quantal  $Ca^{2+}$  release when it occupies all  $IP_3Rs$ , the quantal phenomenon cannot be due to all-or-nothing emptying of stores with heterogeneous sensitivities. The response to a maximal concentration of **2** in Figure 3A is biphasic, and we also observed some biphasic responses to  $IP_3$  (see Figures S5L and S5M), but such biphasic responses were not consistently observed and were not further analyzed.

When cells are maximally stimulated with **2**,  $IP_3$  can bind to  $IP_3R$  only after **2** dissociates. Rapid  $IP_3$ -evoked  $Ca^{2+}$  release after maximal stimulation with **2** (Figures 3E and 3F) therefore demonstrates that quantal  $Ca^{2+}$  release is accompanied by rapid dissociation and re-association of agonists:  $IP_3$  is not “locked” onto activated  $IP_3Rs$ . We conclude that during quantal responses, there is incomplete emptying of the entire ER, and  $IP_3$  continues to associate with and dissociate from  $IP_3Rs$  (Figures 1B and 3G).

### Quantal $Ca^{2+}$ release is not a property of the ER

Since quantal  $Ca^{2+}$  release occurs with  $IP_3Rs$  (Figure 1) (Yamashita, 2006) and RyRs (Cheek et al., 1994; Wang et al., 2004), it might reflect properties of the ER rather than its channels. Increases in  $[Ca^{2+}]_c$  can, for example, restructure the ER (Subramanian and Meyer, 1997), suggesting that loss of  $Ca^{2+}$  from the ER might cause its further fragmentation and deny active  $Ca^{2+}$  channels access to the remaining  $Ca^{2+}$ . Transient receptor potential mucolipin 1 (TRPML1) channels are usually expressed in the membranes of lysosomes (Shen et al., 2012), but when overexpressed TRPML1 channels also release  $Ca^{2+}$  from the ER and some TRPML1 populates the reticular ER in which  $IP_3Rs$  are expressed (Figures 4A and S5A–S5F). In permeabilized HEK cells expressing CFP-TRPML1, but not in mock-transfected cells, ML-SA1 (a selective TRPML1 agonist) (Shen et al., 2012) stimulated a concentration-dependent  $Ca^{2+}$  release from the ER (Figures 4A and S5A). In contrast to the quantal responses evoked by  $IP_3$  and **2**, ML-SA1 caused a concentration-dependent

(F) Summary results (individual values, mean  $\pm$  SEM,  $n = 5$ ) show  $Ca^{2+}$  release (determined at 500 s) evoked by the indicated concentrations of **2** followed by  $IP_3$  in wild-type HEK cells. \*\* $p < 0.01$ , \*\*\* $p < 0.001$ , \*\*\*\* $p < 0.0001$ ; ns, not significant (for indicated comparisons, ANOVA with Bonferroni's test).

(G) Maximal  $IP_3$  concentrations fully empty the  $IP_3$ -sensitive  $Ca^{2+}$  stores, but it was unclear whether quantal responses to submaximal  $IP_3$  concentrations arise from incomplete emptying of the entire ER (i) or complete emptying of a fraction of the ER (ii). Results with a maximally effective concentration of **2**, which partially activates all  $IP_3Rs$  leaving  $Ca^{2+}$  trapped within the ER, indicate that quantal responses are not due to all-or-nothing emptying of heterogeneous stores (ii).



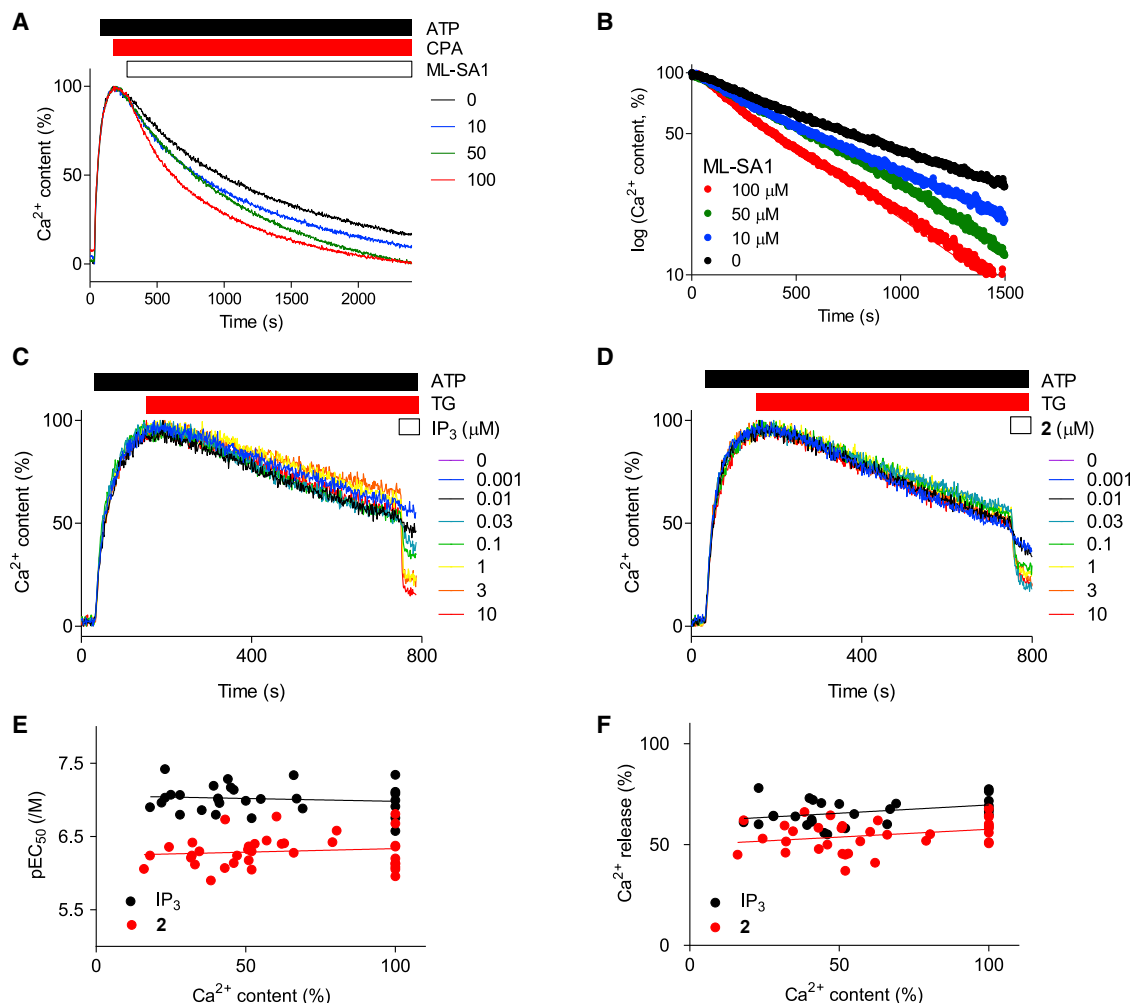


**Figure 4. Neither ER reorganization nor luminal  $\text{Ca}^{2+}$  mediates quantal  $\text{Ca}^{2+}$  release**

(A) Effects of the indicated concentrations of ML-SA1 on the ER  $\text{Ca}^{2+}$  content of permeabilized HEK cells expressing CFP-TRPML1. (B) Semi-logarithmic plots show mono-exponential loss of ER  $\text{Ca}^{2+}$  after treatment with ML-SA1. Results (A and B) are typical of four experiments, each with duplicate determinations. Summary results are in Figure S5B. (C and D) Permeabilized DT40-IP<sub>3</sub>R1 cells were loaded to steady state with  $\text{Ca}^{2+}$  before addition of thapsigargin (TG, 1  $\mu\text{M}$ ) to inhibit SERCAs. At intervals thereafter (0–35 min), IP<sub>3</sub> (C) or **2** (D) was added. Results are typical of 29–36 experiments. (E and F) Summary results (each point from a single concentration-effect relationship) show the relationships between ER  $\text{Ca}^{2+}$  content at the time of addition of IP<sub>3</sub> or **2** (%) and pEC<sub>50</sub> value ( $-\log\text{EC}_{50}$ ) (E) and maximal  $\text{Ca}^{2+}$  release (F). Lines (least-squares linear regression) have slopes that are not significantly different from 0. See also Figure S5.

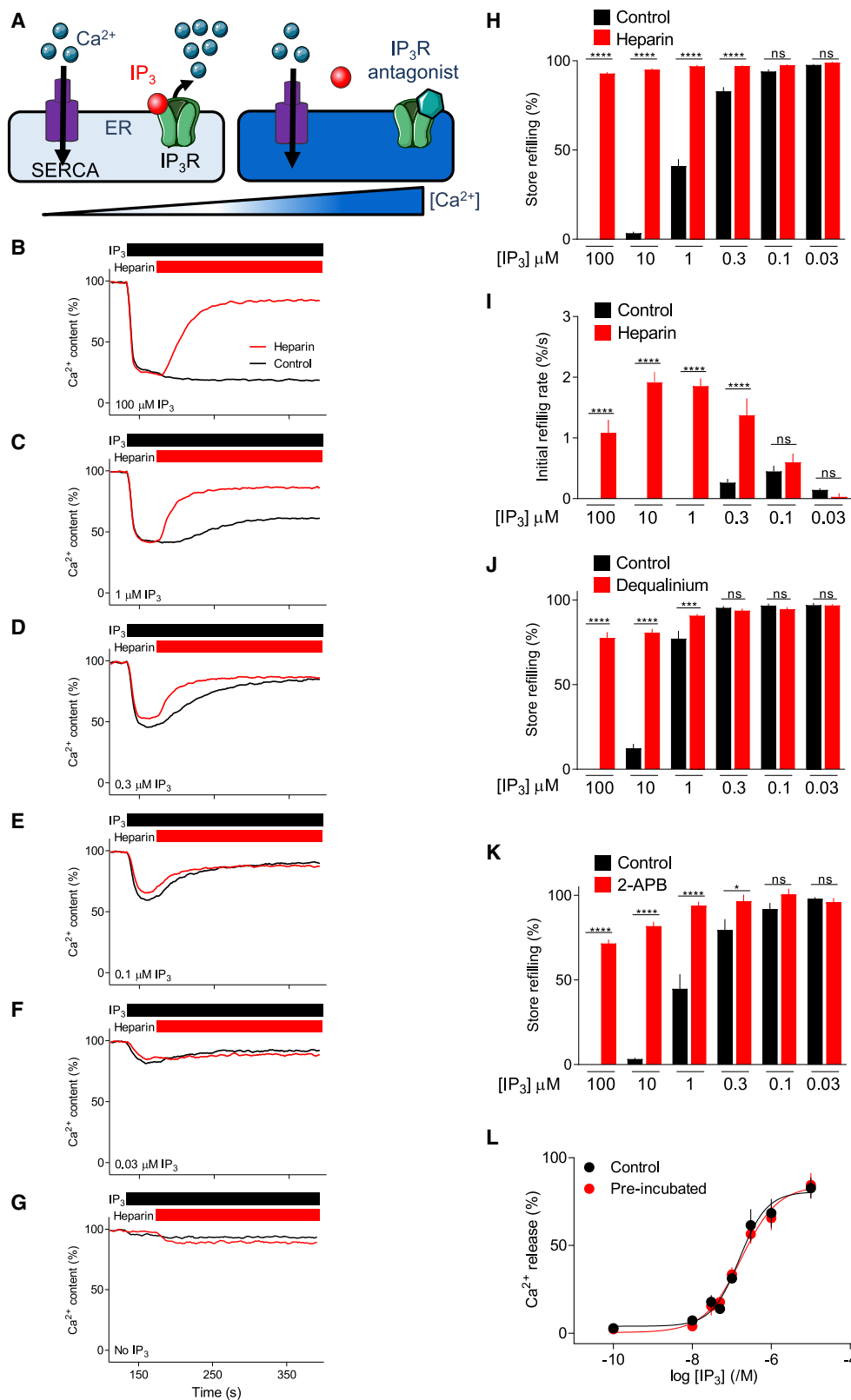
increase in the rate of  $\text{Ca}^{2+}$  release from the entire ML-SA1-sensitive ER (Figures 4B and S5B). These results establish that quantal  $\text{Ca}^{2+}$  release is not a property of the ER or an inexorable consequence of cell permeabilization with the associated ER fragmentation (Figure S4O), but it is instead a feature of IP<sub>3</sub>Rs and RyRs. That conclusion is consistent with evidence that purified IP<sub>3</sub>Rs mediate quantal  $\text{Ca}^{2+}$  release (Ferris et al., 1992).

#### Neither luminal $\text{Ca}^{2+}$ nor erlin 2 determines quantal responses

An appealing hypothesis is that luminal  $\text{Ca}^{2+}$  is required for IP<sub>3</sub>R gating, such that as the ER loses  $\text{Ca}^{2+}$  the IP<sub>3</sub>R channel closes

trapping  $\text{Ca}^{2+}$  within the ER (Irvine, 1990) (Figure 1C). Previous analyses of the effects of luminal  $\text{Ca}^{2+}$  provide conflicting results. There is evidence that a very substantial loss of ER  $\text{Ca}^{2+}$  reduces IP<sub>3</sub>R sensitivity (Barrero et al., 1997; Marshall and Taylor, 1994) and that overloading stores with  $\text{Ca}^{2+}$  promotes  $\text{Ca}^{2+}$  release (Missiaen et al., 1992), while other reports suggest that luminal  $\text{Ca}^{2+}$  reduces IP<sub>3</sub>R sensitivity (Vais et al., 2020) or has no effect (Beecroft and Taylor, 1997; Shuttleworth, 1992).

We anticipated that if three ligands are required to open IP<sub>3</sub>Rs (IP<sub>3</sub>, cytosolic  $\text{Ca}^{2+}$ , and luminal  $\text{Ca}^{2+}$ , Figure 1C), channel opening by IP<sub>3</sub> might require less luminal  $\text{Ca}^{2+}$  than the weak partial agonist **2**. We used thapsigargin to irreversibly inhibit SERCA



(legend on next page)

and slowly drain the ER of  $\text{Ca}^{2+}$ , and then evaluated responses to  $\text{IP}_3$  and **2** at different ER  $\text{Ca}^{2+}$  contents (Figures 4C and 4D). The fraction of the remaining  $\text{Ca}^{2+}$  stores released by  $\text{IP}_3$  or **2** and the  $\text{EC}_{50}$  for each ligand were unaffected as stores lost their  $\text{Ca}^{2+}$ . We conclude that there is no significant effect of ER  $\text{Ca}^{2+}$  content on the sensitivity or maximal response to  $\text{IP}_3$  or **2** (Figures 4E and 4F), even when the  $\text{Ca}^{2+}$  content is reduced to levels well below those observed after quantal responses to  $\text{IP}_3$  or **2**. Luminal  $\text{Ca}^{2+}$  does not, therefore, affect the number of open  $\text{IP}_3\text{Rs}$ . We conclude, and consistent with some previous reports (Beecroft and Taylor, 1997; Combettes et al., 1992; Hajnóczky and Thomas, 1994; Oldershaw et al., 1991; Shuttleworth, 1992), that regulation of  $\text{IP}_3\text{Rs}$  by luminal  $\text{Ca}^{2+}$  does not underlie quantal responses.

Activation of  $\text{IP}_3\text{Rs}$  initiates a sequence that can lead to their proteasomal degradation. An early step in this sequence is recognition of active  $\text{IP}_3\text{Rs}$  by an ER-membrane protein, erlin 2 (ER lipid raft-associated protein 2) (Wojcikiewicz, 2018). We considered whether erlin 2 might associate with active  $\text{IP}_3\text{Rs}$ , terminate their activity, and thereby contribute to quantal  $\text{Ca}^{2+}$  release. However, substantial depletion of erlin 2 using small interfering RNA (siRNA) had no effect on quantal responses to  $\text{IP}_3$  (Figures S5G–S5M). We conclude that neither erlin 2 nor changes in ER luminal  $[\text{Ca}^{2+}]$  contribute to incremental  $\text{Ca}^{2+}$  release by  $\text{IP}_3$ .

### **$\text{IP}_3$ evokes $\text{Ca}^{2+}$ release and then $\text{IP}_3\text{R}$ inactivation**

Previous analyses of  $\text{IP}_3\text{R}$  inactivation provide conflicting results, perhaps indicating a need for unidentified labile accessory factors (Bezprozvanny and Ehrlich, 1994; Hajnóczky and Thomas, 1994; Mak and Foskett, 1997; Marchant and Taylor, 1998; Oldershaw et al., 1992; Taufiq-Ur-Rahman et al., 2009; Stehno-Bittel et al., 1995). To examine any possible contribution of  $\text{IP}_3\text{R}$  inactivation to quantal  $\text{Ca}^{2+}$  release, we therefore examined  $\text{IP}_3\text{R}$  inactivation under conditions that exactly replicate those we used to show incremental responses to  $\text{IP}_3$ .

To assess the activity of  $\text{IP}_3\text{Rs}$  during the sustained phase of incremental responses, we examined  $\text{IP}_3$ -evoked  $\text{Ca}^{2+}$  release without inhibiting SERCAs and then added an  $\text{IP}_3\text{R}$  antagonist during the response. The rationale is that if  $\text{IP}_3\text{Rs}$  remain active, an antagonist should reverse any ongoing activity and allow stores to refill (Figure 5A). We used three unrelated antagonists since each has limitations (Figure S6). Heparin is a competitive

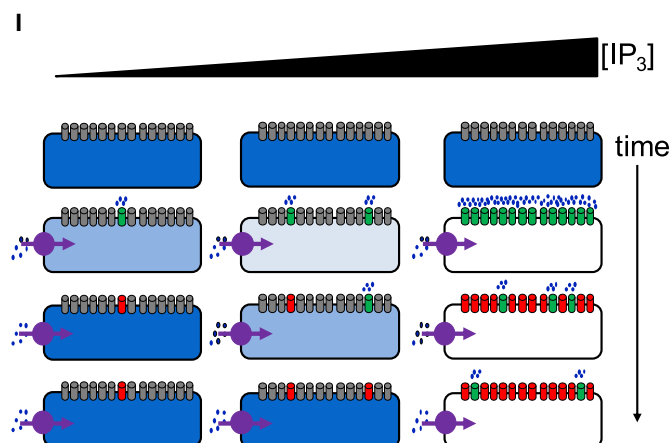
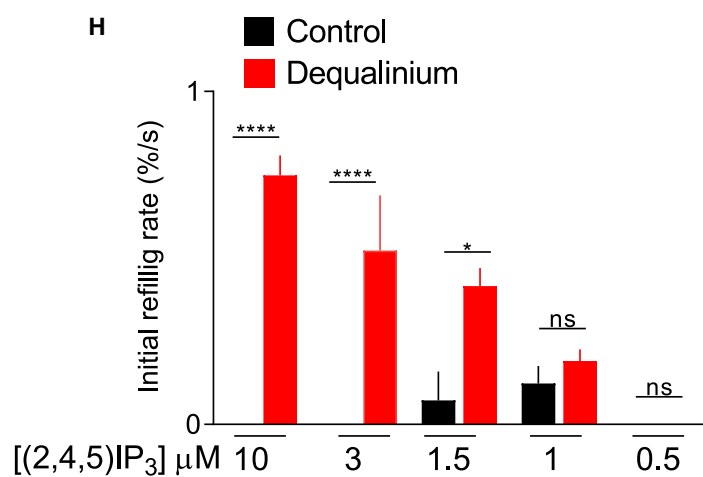
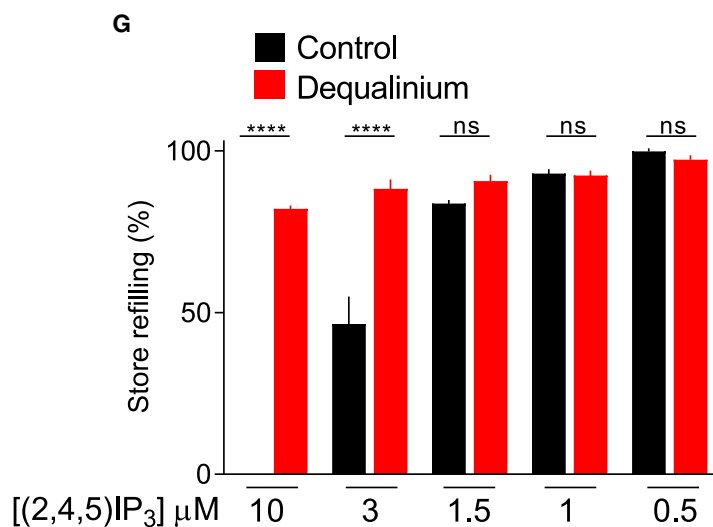
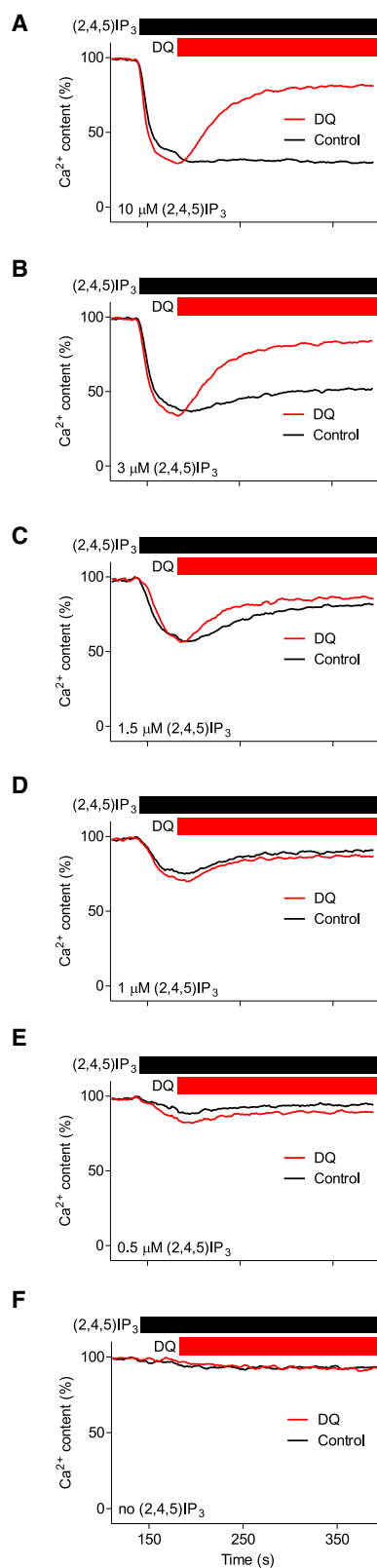
antagonist (Richardson and Taylor, 1993) and 2-aminoethoxydiphenyl borate (2-APB) is a non-competitive inhibitor with some selectivity for  $\text{IP}_3\text{R1}$  (Saleem et al., 2014). We show that dequalinium, which blocks  $\text{K}^+$  channels, is also an  $\text{IP}_3\text{R}$  antagonist (Figures S6A–S6G). At the concentrations used, the antagonists completely (heparin and dequalinium) or partially (2-APB) blocked  $\text{IP}_3$ -evoked  $\text{Ca}^{2+}$  release from permeabilized HEK- $\text{IP}_3\text{R1}$  cells (Figures S6H–S6J).

During sustained stimulation of permeabilized HEK- $\text{IP}_3\text{R1}$  cells with a maximal concentration of  $\text{IP}_3$ , the stores remained empty, but they refilled after adding heparin (Figure 5B). The incomplete refilling is probably due to partial inhibition of SERCAs by heparin (Figures S6K–S6M). The results demonstrate that during maximal stimulation, enough  $\text{IP}_3\text{Rs}$  remain open to counteract opposing SERCA activity. Since an  $\text{IP}_3\text{R}$  can conduct  $\sim 500,000 \text{ Ca}^{2+}/\text{s}$  (Vais et al., 2010) while a SERCA transports fewer than  $40 \text{ Ca}^{2+}/\text{s}$  (Lytton et al., 1992), it may require very little residual  $\text{IP}_3\text{R}$  activity to overwhelm SERCAs and keep the ER depleted of  $\text{Ca}^{2+}$ . After stimulation with the lowest  $\text{IP}_3$  concentrations (30–100 nM), the stores rapidly refilled and the rate was unaffected by heparin (Figures 5E–5I). This indicates that after the initial  $\text{Ca}^{2+}$  release evoked by low  $\text{IP}_3$  concentrations, there were no detectable open  $\text{IP}_3\text{Rs}$ . The pattern of response to intermediate concentrations of  $\text{IP}_3$  fell between these extremes: there was residual sustained  $\text{IP}_3\text{R}$  activity with the higher  $\text{IP}_3$  concentrations, and  $\text{IP}_3\text{R}$  inactivation occurred with the lower concentrations, but more slowly than for the lowest  $\text{IP}_3$  concentration (Figures 5C, 5D, 5H, and 5I). Similar results were obtained with different antagonists (Figures 5J, 5K, and S7), with heparin in wild-type HEK cells (Figures S7M–S7T), and with a metabolically stable analog of  $\text{IP}_3$ , (2,4,5) $\text{IP}_3$  (Figures 6A–6H). We also used a bioassay of  $\text{IP}_3$  to confirm that refilling of  $\text{Ca}^{2+}$  stores during prolonged incubation with low concentrations of  $\text{IP}_3$  was not due to  $\text{IP}_3$  degradation (Figure 5L; Table S4).

Previous studies provide conflicting evidence for  $\text{IP}_3$ -evoked  $\text{IP}_3\text{R}$  inactivation. Single-channel recordings of  $\text{IP}_3\text{Rs}$  support (Mak and Foskett, 1997; Stehno-Bittel et al., 1995) or challenge inactivation (Bezprozvanny and Ehrlich, 1994; Taufiq-Ur-Rahman et al., 2009), and while some analyses of permeabilized cells show  $\text{IP}_3$ -evoked inactivation (Hajnóczky and Thomas, 1994; Marchant and Taylor, 1998), others suggest that responses are

### **Figure 5. $\text{IP}_3\text{Rs}$ close after rapid $\text{Ca}^{2+}$ release evoked by low $\text{IP}_3$ concentrations**

(A) If  $\text{IP}_3\text{Rs}$  remain active after an incremental  $\text{Ca}^{2+}$  release; stores should re-accumulate  $\text{Ca}^{2+}$  after addition of an  $\text{IP}_3\text{R}$  antagonist.  
(B–G) The ER of permeabilized HEK- $\text{IP}_3\text{R1}$  cells was loaded with  $\text{Ca}^{2+}$  by addition of ATP ( $t = 0$ );  $\text{IP}_3$  (0–30  $\mu\text{M}$ ) and heparin (10 mg/mL) were then added as indicated. Each trace (mean of duplicate determinations) shows results with a different  $\text{IP}_3$  concentration. The code in (B) applies to all panels.  
(H and I) Summary results (mean  $\pm$  SEM,  $n = 6$ , each with two determinations) show the extent to which stores have refilled (relative to cells without  $\text{IP}_3$ ) 250 s after  $\text{IP}_3$  addition (H), as well as the initial rate of refilling from the slope of the curve immediately after heparin addition (I). In (H), 0% refilling is defined as the store content in control conditions measured 250 s after addition of a maximal  $\text{IP}_3$  concentration. In these experiments, the  $\text{EC}_{50}$  for  $\text{IP}_3$ -evoked  $\text{Ca}^{2+}$  release was 166 nM ( $\text{pEC}_{50} = 6.78 \pm 0.08$ ) and maximal  $\text{Ca}^{2+}$  release was  $86\% \pm 2\%$  (mean  $\pm$  SEM,  $n = 6$ ).  
(J and K) Summary results (mean  $\pm$  SEM,  $n = 5$ –7, each with two determinations) from similar analyses using 50  $\mu\text{M}$  dequalinium (J; Figures S7A–S7F) or 125  $\mu\text{M}$  2-APB (K; Figures S7G–S7L) to block  $\text{IP}_3\text{Rs}$ . \* $p < 0.05$ , \*\*\* $p < 0.001$ , \*\*\*\* $p < 0.0001$ , one-way repeated ANOVA with Bonferroni's test for the indicated comparisons (H–K).  
(L)  $\text{IP}_3$  was incubated with permeabilized HEK- $\text{IP}_3\text{R1}$  cells (pre-incubated) or without cells (control) for 260 s under conditions identical to those used to show  $\text{IP}_3\text{R}$  inactivation. The supernatant was then bio-assayed. Summary results (mean  $\pm$  SEM,  $n = 4$ , each with three replicates) show no significant difference between the potency of  $\text{IP}_3$  after incubation under control conditions or with permeabilized cells. The results establish that refilling of stores during sustained incubation with low concentrations of  $\text{IP}_3$  is not due to its metabolism. Table S4 provides a summary and detailed methods.  
See also Figures S6 and S7 and Table S4.



(legend on next page)

sustained (Oldershaw et al., 1992). Our results, from analyses where incremental responses and inactivation were assessed under identical conditions, show that incremental responses to low IP<sub>3</sub> concentrations are accompanied by rapid inactivation of IP<sub>3</sub>Rs (Figure 6I).

### Incremental responses involve activation of very few IP<sub>3</sub>Rs

If quantal responses to low IP<sub>3</sub> concentrations are terminated by closure of IP<sub>3</sub>Rs, how can stores retain undiminished responsiveness to further IP<sub>3</sub> additions? Comparison of the relationship between the occupancy of IP<sub>3</sub>Rs by IP<sub>3</sub> with functional responses provides a possible answer to this conundrum.

Analyses of [<sup>3</sup>H]IP<sub>3</sub> binding establish the fraction of IP<sub>3</sub>-binding sites to which each concentration of IP<sub>3</sub> has bound ( $\alpha$ ) without revealing how the binding is distributed between IP<sub>3</sub>Rs or their different states. However, Hill coefficients for IP<sub>3</sub> binding to IP<sub>3</sub>R1 are close to one ( $0.95 \pm 0.08$  in Figure 2B) (Hannaert-Merah et al., 1994; Iwai et al., 2005; Rossi et al., 2009; Supattapone et al., 1988), indicating that each IP<sub>3</sub>R subunit binds IP<sub>3</sub> independently (Hannaert-Merah et al., 1994) and that differences in the affinities of different IP<sub>3</sub>R states are either small or masked by the predominance of a single state. We therefore assume that IP<sub>3</sub> binding is independently distributed across all available IP<sub>3</sub>-binding sites. Since IP<sub>3</sub>R opening requires binding of IP<sub>3</sub> to all four IP<sub>3</sub>R subunits (Alzayady et al., 2016), we need to predict the relationship between IP<sub>3</sub> concentration and the fraction of IP<sub>3</sub>R with all four sites occupied ( $\alpha^4$ , Figure 7A). We begin with analyses of HEK-IP<sub>3</sub>R1 cells.

Our measurements of IP<sub>3</sub>-evoked Ca<sup>2+</sup> release lack the temporal resolution needed to determine the initial rates of Ca<sup>2+</sup> release that would directly report the number of open IP<sub>3</sub>Rs (Marchant and Taylor, 1998). However, the assays do establish the IP<sub>3</sub> sensitivity of quantal responses, because (with SERCAs inhibited) the Ca<sup>2+</sup> release determined after 20 s for each IP<sub>3</sub> concentration reports the cumulative response to IP<sub>3</sub> throughout that interval. When addressing mechanisms of quantal Ca<sup>2+</sup> release, it is, therefore, appropriate to compare the sensitivity to IP<sub>3</sub> of quantal Ca<sup>2+</sup> release (the fraction of Ca<sup>2+</sup> stores released) to estimates of how many IP<sub>3</sub>Rs are likely to be tetra-liganded by that concentration of IP<sub>3</sub>. We used IP<sub>3</sub>R1 from cerebellum ( $2.75 \times 10^8$  IP<sub>3</sub>Rs/ $\mu$ L of sample, determined from [<sup>3</sup>H]IP<sub>3</sub> binding) to calibrate western blots, and so determine the number of IP<sub>3</sub>Rs in HEK-IP<sub>3</sub>R1 cells ( $49,146 \pm 15,001$  IP<sub>3</sub>Rs/cell) (Figure 7B). Comparing the affinity of IP<sub>3</sub>R1 for IP<sub>3</sub> under conditions that replicate functional assays (Figure 2G) with the number of IP<sub>3</sub>Rs in HEK-IP<sub>3</sub>R1 cells, we predict that the Ca<sup>2+</sup> release evoked by a half-maximally effective

concentration of IP<sub>3</sub> is associated with opening of only 0.13% of a cell's IP<sub>3</sub>Rs, or about 60 IP<sub>3</sub>Rs/cell (Figures 7C and 7D). This situation, where only a tiny fraction of available receptors elicits a response, is analogous to the "spare receptors" found in many signaling pathways initiated by plasma membrane receptors. Here, all receptors are competent to respond, but there are many more receptors than required to elicit a maximal response (Stephenson, 1956). Our argument does not require an additional level of IP<sub>3</sub>R regulation, although that may also occur (Thillaiappan et al., 2017; Thillaiappan et al., 2021); it requires only that cells express more IP<sub>3</sub>Rs than are needed to deplete the ER of Ca<sup>2+</sup>. In analogy with spare receptors elsewhere, we expect this feature to increase the sensitivity of Ca<sup>2+</sup> release to IP<sub>3</sub>.

An open IP<sub>3</sub>R is predicted to mediate movement of about 500,000 Ca<sup>2+</sup>/s out of the ER (Vais et al., 2010). We estimate the ER Ca<sup>2+</sup> content of a single permeabilized HEK cell to be about  $9 \times 10^{-16}$  mol (see *Simulations* in STAR Methods). This suggests that sustained opening of a single IP<sub>3</sub>R for the 20 s taken for incremental responses to plateau would be sufficient to cause loss of almost 2% of the ER Ca<sup>2+</sup> content of a cell. The key point is that very few of the many IP<sub>3</sub>Rs in a cell are active during incremental responses to IP<sub>3</sub> and they are sufficient to account for the observed responses (Figure 7D).

### A mechanism for incremental responses to IP<sub>3</sub>

We propose that after IP<sub>3</sub> addition, very few of the many IP<sub>3</sub>Rs in a cell rapidly bind IP<sub>3</sub> to each of their four subunits; many more IP<sub>3</sub>Rs will be partially occupied (Figures 7A, 7C, and 7D). The fully occupied IP<sub>3</sub>Rs open and rapidly release Ca<sup>2+</sup>; they then inactivate and more slowly recover (Figure 7E). After the initial Ca<sup>2+</sup> release, when activation of IP<sub>3</sub>Rs is effectively synchronized by IP<sub>3</sub> addition, additional IP<sub>3</sub>Rs will open as they bind four IP<sub>3</sub> molecules and then proceed to inactivate, but their openings will be asynchronous. Hence, addition of IP<sub>3</sub> drives a few IP<sub>3</sub>Rs through a near-synchronous sequence of opening and inactivation, after which very small numbers of IP<sub>3</sub>Rs proceed through the sequence asynchronously. The next step in IP<sub>3</sub> concentration then drives another pulse of near-synchronous IP<sub>3</sub>R openings.

Two features of this scheme contribute to understanding incremental responses. First, incremental responses are mediated by only a tiny fraction of the IP<sub>3</sub>Rs in a cell (<1%, Figures 7C and 7D). Inactivation therefore negligibly impacts the number of IP<sub>3</sub>Rs available for subsequent activation, ensuring that despite some inactivation of IP<sub>3</sub>Rs, responses to subsequent IP<sub>3</sub> additions are unperturbed. Second, because IP<sub>3</sub>Rs move inexorably from an open to an inactivated state, there will always be more open IP<sub>3</sub>Rs immediately after an IP<sub>3</sub> addition (when openings

### Figure 6. IP<sub>3</sub>Rs of HEK-IP<sub>3</sub>R1 cells close after incremental responses to low concentrations of a stable analog of IP<sub>3</sub>

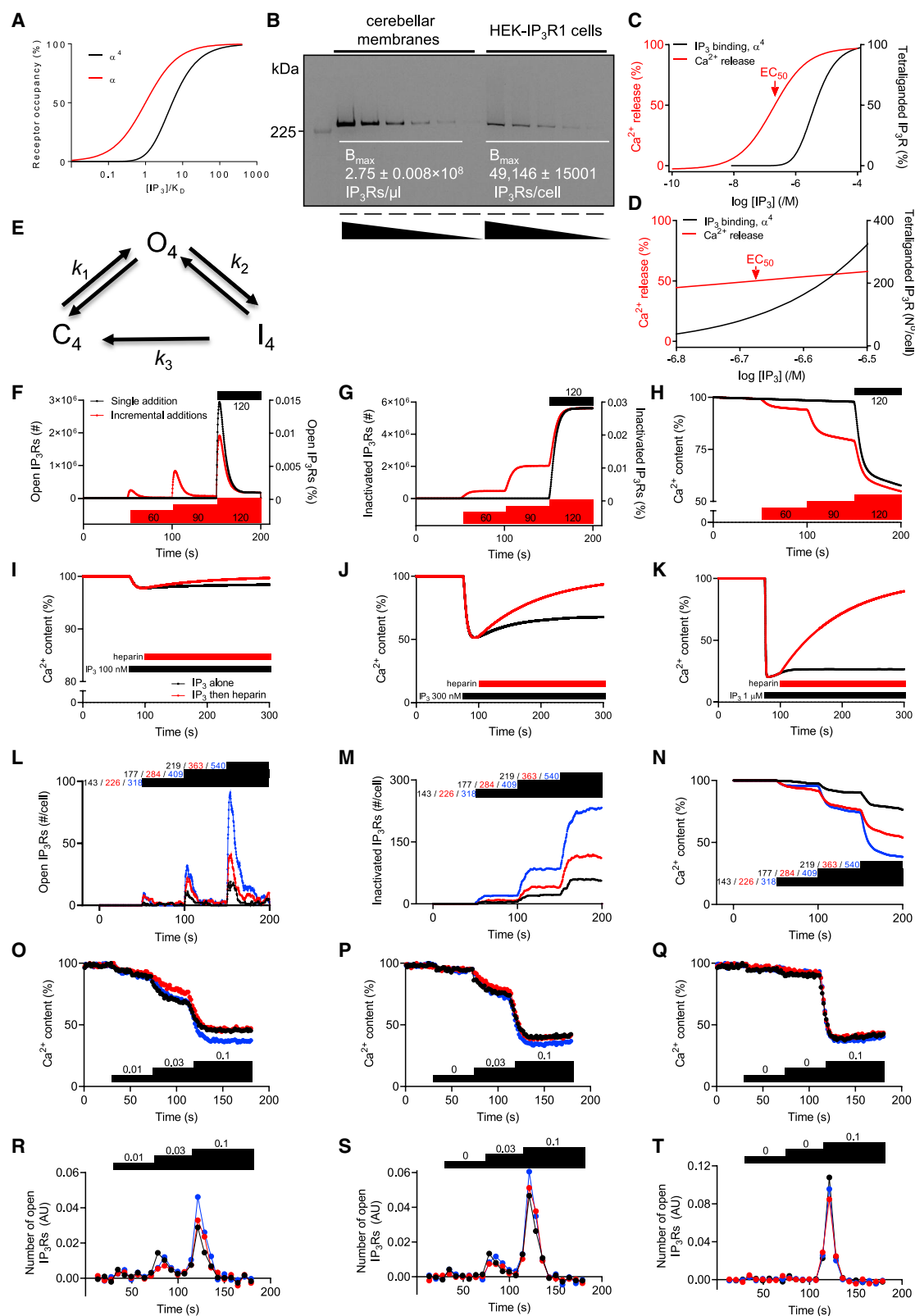
(A–F) The experiments are similar to those shown in Figure 5, but using HEK-IP<sub>3</sub>R1 cells, (2,4,5)IP<sub>3</sub> at the indicated concentrations, and dequalinium (DQ, 50  $\mu$ M). Permeabilized cells were loaded with Ca<sup>2+</sup> by addition of ATP before adding the indicated concentrations of (2,4,5)IP<sub>3</sub> (without inhibiting SERCAs) and then the IP<sub>3</sub>R antagonist, dequalinium. Traces show means of two replicates.

(G and H) Summary results (mean  $\pm$  SEM, n = 4, each with two determinations) show the extent to which stores refill (relative to cells without (2,4,5)IP<sub>3</sub>) 250 s after (2,4,5)IP<sub>3</sub> addition (G), and the initial rate of refilling from the slope of the curve immediately after DQ addition (H). \*p < 0.05, \*\*\*\*p < 0.0001, one-way ANOVA with Bonferroni's test.

(I) Stores rapidly refill after stimulation with the lowest IP<sub>3</sub> concentrations, as the very few active IP<sub>3</sub>Rs inactivate. Higher concentrations of IP<sub>3</sub> activate many more IP<sub>3</sub>Rs than needed to empty the stores, hence even substantial inactivation leaves enough active IP<sub>3</sub>Rs to keep the stores empty.

See also Figures S6 and S7.





(legend on next page)

are synchronized) than later (when IP<sub>3</sub>Rs progress to inactivated states) (Figure 7E). A surge of Ca<sup>2+</sup> release after each IP<sub>3</sub> addition is followed by a period of much reduced activity, thereby explaining the quantal pattern of Ca<sup>2+</sup> release.

There is evidence, albeit with conflicting observations, that rapid activation of IP<sub>3</sub>Rs by IP<sub>3</sub> is followed by slower inactivation (half-time [ $t_{1/2}$ ] of about 15–30 s) (Hajnóczky and Thomas, 1994; Mak et al., 2000, 2001; Stehno-Bittel et al., 1995) and even slower recovery ( $t_{1/2}$  of 30 s to several minutes) (Hajnóczky and Thomas, 1994; Ionescu et al., 2006). This mechanism would allow incremental responses only if inactivation requires most (probably all four) IP<sub>3</sub>-binding sites to be occupied; otherwise, IP<sub>3</sub>Rs would inactivate before they opened. An alternative mechanism is “feed-through” inhibition of IP<sub>3</sub>Rs by Ca<sup>2+</sup> as it passes through an open channel (Dawson et al., 2003), but even these very local Ca<sup>2+</sup> signals would probably be intercepted by 10 mM BAPTA (Vais et al., 2012), which did not prevent quantal responses (Figures S2A–S2F). We suggest that IP<sub>3</sub>R inactivation is directly linked to activation rather than via feedback effects from increased [Ca<sup>2+</sup>]<sub>c</sub>.

### A simple activation-inactivation scheme predicts incremental responses to IP<sub>3</sub>

We developed an empirical scheme with stochastic simulations to assess whether it captured key features of the experimental observations. A simplified scheme is needed to reduce computation times for the stochastic simulations of the many IP<sub>3</sub>Rs required to address the consequences of a few IP<sub>3</sub>Rs opening

together and then losing synchrony as they inactivate. The scheme envisages that an IP<sub>3</sub>R opens rapidly ( $t_{1/2}$  of ~2.5 s) after it has bound four molecules of IP<sub>3</sub>, before slowly inactivating ( $t_{1/2}$  of ~5 s) and then very slowly recovering from the inactivated to the closed state ( $t_{1/2}$  of ~250 s) (Figure 7E). The detailed mechanisms of IP<sub>3</sub>-evoked IP<sub>3</sub>R inactivation are unresolved and may require interaction with additional unidentified molecules. Hence, our empirical scheme based on the activation-inactivation sequence shown in Figure 7E is not a closed cycle (see Simulations in STAR Methods).

Mathematical simulations using our simplified scheme (Figure 7E) and with the numbers of IP<sub>3</sub>Rs determined in functional analyses of HEK-IP<sub>3</sub>R1 cells in 96-well plates ( $4 \times 10^5$  cells/well,  $\sim 2 \times 10^{10}$  IP<sub>3</sub>Rs/well) (Figure 7B) capture the key experimental observations. Each addition of a submaximal IP<sub>3</sub> concentration evokes a surge of IP<sub>3</sub>R openings followed by stable inactivation of a small fraction of the IP<sub>3</sub>R population. The ER Ca<sup>2+</sup> content responds incrementally to successive IP<sub>3</sub> additions. Finally, with SERCAs active, stores rapidly refill in the presence of low IP<sub>3</sub> concentrations, but remain depleted with higher concentrations (Figures 7F–7K).

Most of our analyses used populations of cells in 96-well plates, but incremental responses to IP<sub>3</sub> are also evident in single wild-type HEK cells (Figures S4J–S4N). We therefore measured the number of IP<sub>3</sub>Rs in wild-type HEK cells ( $9,101 \pm 934$  IP<sub>3</sub>Rs/cell, mean  $\pm$  SD,  $n = 3$ ) and applied our scheme to a single cell. The simulations confirm that here too, the scheme predicts behavior consistent with experimental observations. Incremental additions

### Figure 7. Incremental responses are mediated by very few IP<sub>3</sub>Rs that rapidly inactivate

(A) IP<sub>3</sub> must bind to all four IP<sub>3</sub>-binding sites of a tetrameric IP<sub>3</sub>R for the channel to open (Alzayady et al., 2016). Since IP<sub>3</sub> binds independently to each site and with the same  $K_D$ , we compute the fractional occupancy of all IP<sub>3</sub>-binding sites ( $\alpha$ ) at any ligand concentration ( $[L]$ ) from:  $\alpha = ([L]/K_D) / (1 + [L]/K_D)$ . The fraction of tetrameric IP<sub>3</sub>R in which all four sites are occupied is then  $\alpha^4$ . The plot shows the relationship between normalized ligand concentration ( $[L]/K_D$ ) and the fraction of IP<sub>3</sub>Rs in which all four IP<sub>3</sub>-bindings sites are occupied ( $\alpha^4$ ) compared to the fractional occupancy at a single site ( $\alpha$ ).

(B) Equilibrium competition binding with [<sup>3</sup>H]IP<sub>3</sub> in TEM was used to define the  $K_D$  and from that the maximal number of binding sites ( $B_{max}$ ) in cerebellar membranes, which were then used to calibrate western blots to estimate the number of IP<sub>3</sub>Rs in a HEK-IP<sub>3</sub>R1 cell. Loadings are for serial 2-fold dilutions from 3.2 to 0.1  $\mu$ L/lane (cerebellum) and from 12.8 to 0.8  $\mu$ L/lane (HEK-IP<sub>3</sub>R1 cells). The HEK-IP<sub>3</sub>R1 cell lysate contained 10,000 cells/ $\mu$ L.  $B_{max}$  values are mean  $\pm$  SEM,  $n = 6$ .

(C) Predicted relationship for HEK-IP<sub>3</sub>R1 cells between IP<sub>3</sub> concentration, number of IP<sub>3</sub>Rs (% of total) with all four IP<sub>3</sub>-binding sites occupied (calculated from the  $K_D$  for IP<sub>3</sub> determined under conditions used for functional assays, 794 nM), and IP<sub>3</sub>-evoked Ca<sup>2+</sup> release (% of IP<sub>3</sub>-sensitive stores;  $EC_{50} = 186$  nM,  $pEC_{50} = 6.73 \pm 0.04$ ;  $n = 17$ ).

(D) Relationships between IP<sub>3</sub> concentrations around the  $EC_{50}$  value, Ca<sup>2+</sup> release, and the number of tetra-liganded IP<sub>3</sub>Rs/cell.

(E) We assume that IP<sub>3</sub>Rs in which four subunits have bound IP<sub>3</sub> move between closed ( $C_4$ ), open ( $O_4$ ), and inactivated ( $I_4$ ) states with forward rate constants  $k_1 > k_2 \gg k_3$ .

(F–H) Simulations show numbers of open (F) and inactivated IP<sub>3</sub>Rs/well (G), and the ER Ca<sup>2+</sup> content (H) for HEK-IP<sub>3</sub>R1 cells after sequential additions to give the indicated final IP<sub>3</sub> concentrations (nM) or a single addition of the final IP<sub>3</sub> concentration. Each addition of IP<sub>3</sub> evokes a rapid, transient surge in the number of open IP<sub>3</sub>Rs, which then rapidly inactivate, leading to transient Ca<sup>2+</sup> release. Note the tiny fraction of open and inactivated IP<sub>3</sub>Rs (right axes in F and G).

(I–K) Simulations for HEK-IP<sub>3</sub>R1 cells with SERCAs active show ER Ca<sup>2+</sup> content after addition of the indicated IP<sub>3</sub> concentrations and then heparin (similar to analyses in Figures 5 and 6). Addition of heparin was simulated by making  $k_{rel} = 0$ .

(L–N) In the simulations of cell populations (F–H), stepwise increases in IP<sub>3</sub> concentration caused the predicted number of tetra-liganded IP<sub>3</sub>Rs (IP<sub>3</sub>R<sup>4</sup>) to increase by 4.41-fold (for 60 to 90 nM) and then by 2.76-fold (90 to 120 nM). Here, we simulate responses from a single wild-type HEK cell expressing 9,101 IP<sub>3</sub>Rs, with the first IP<sub>3</sub> addition triggering formation of 5 IP<sub>3</sub>R<sup>4</sup>s/cell (143 nM), 10 IP<sub>3</sub>R<sup>4</sup>s/cell (177 nM), or 20 IP<sub>3</sub>R<sup>4</sup>s/cell (219 nM). We then deliver two further IP<sub>3</sub> additions calculated to cause the numbers of IP<sub>3</sub>R<sup>4</sup>s to increase by 4.41-fold and then by 2.76-fold to mimic the stimuli used in simulations of larger numbers of cells (F–G). Simulations show the effects of adding the indicated concentrations of IP<sub>3</sub> on the number of open (L) and inactivated IP<sub>3</sub>Rs (M), and the Ca<sup>2+</sup> content of the ER (N). Colored code indicates concentrations of IP<sub>3</sub> (nM) added at each step.

(O–T) We predict the number of open IP<sub>3</sub>Rs during incremental responses of permeabilized DT40-IP<sub>3</sub>R1 cells by subtracting the ER Ca<sup>2+</sup> leak after inhibition of SERCA (Figure 1D, purple trace) from the results obtained with incremental additions of IP<sub>3</sub> (Figures 1G–1H), and then estimate the time-dependent loss of ER Ca<sup>2+</sup> due to opening of IP<sub>3</sub>Rs (see Analysis in STAR Methods). For each sequence of IP<sub>3</sub> additions, results are shown for each of three independent analyses (blue, red, and black). The results show that after each IP<sub>3</sub> addition, IP<sub>3</sub>Rs abruptly open and then close (inactivate), and the time course of the number of open IP<sub>3</sub>Rs matches predictions of the simple activation-inactivation scheme (F–H), confirming that our scheme captures essential features of IP<sub>3</sub>Rs responding incrementally to IP<sub>3</sub>.

of IP<sub>3</sub> evoke graded loss of ER Ca<sup>2+</sup>, which is associated with transient opening of very small numbers of IP<sub>3</sub>Rs and sustained inactivation of a few IP<sub>3</sub>Rs (Figures 7L–7N).

We also compared the activation-inactivation scheme with experimental data from DT40-IP<sub>3</sub>R1 cells responding incrementally to IP<sub>3</sub> (Figures 1G–1J). Using the experimental data, we identified the component of ER Ca<sup>2+</sup> release attributable to open IP<sub>3</sub>Rs by subtracting the basal IP<sub>3</sub>-independent Ca<sup>2+</sup> leak (see Analysis in STAR Methods). By dividing this IP<sub>3</sub>R-dependent Ca<sup>2+</sup> flux by the time-matched ER Ca<sup>2+</sup> content, we estimated the time course of the number of open IP<sub>3</sub>Rs (in arbitrary numbers) during sequential additions of IP<sub>3</sub> (Figures 7O–7T). The analysis establishes that IP<sub>3</sub>Rs must close within about 10 s of each IP<sub>3</sub> addition. Furthermore, the close correspondence of the time course of IP<sub>3</sub>R openings in the experimental analysis with the predictions of our simple, albeit incomplete, activation-inactivation scheme (Figure 7E) confirms that the scheme captures all essential features of the experimental observations.

## Conclusions

Quantal Ca<sup>2+</sup> release is an unusual feature of IP<sub>3</sub>Rs, first described in 1989 (Muallem et al., 1989), but never adequately explained (Yamashita, 2006). We confirmed that in both intact and permeabilized cells and under conditions where SERCAs cannot counteract IP<sub>3</sub>R activity, submaximal concentrations of IP<sub>3</sub> rapidly release only a fraction of the ER Ca<sup>2+</sup> stores without compromising responses to further incremental IP<sub>3</sub> additions. These features are properties of all three IP<sub>3</sub>R subtypes; they are evident in single cells; they do not arise from ineffective charge compensation during electrogenic Ca<sup>2+</sup> efflux, IP<sub>3</sub> metabolism, increases in [Ca<sup>2+</sup>]<sub>c</sub>, or mitochondrial activity; and they are a property of IP<sub>3</sub>Rs rather than the ER.

We developed a synthetic high-affinity agonist of IP<sub>3</sub>Rs with very low efficacy, **2**, to distinguish between the mechanisms proposed to explain quantal Ca<sup>2+</sup> release (Figures 1A and 1B); **2** has the lowest efficacy reported for any high-affinity agonist of IP<sub>3</sub>R. We used **2** to show that quantal responses do not arise from all-or-nothing emptying of heterogeneous Ca<sup>2+</sup> stores. We do not exclude the possibility that IP<sub>3</sub>Rs within a cell may differ in their IP<sub>3</sub> sensitivity, but it is clear that any such heterogeneity is not required for quantal responses (Figure 3). Instead, after the initial rapid Ca<sup>2+</sup> release evoked by low concentrations of IP<sub>3</sub>, IP<sub>3</sub>Rs close with Ca<sup>2+</sup> still trapped in the ER. Neither erlin 2, an increase in [Ca<sup>2+</sup>]<sub>c</sub>, nor a decrease in ER luminal [Ca<sup>2+</sup>] contributes to this IP<sub>3</sub>R inactivation. Instead, inactivation is probably an inexorable consequence of IP<sub>3</sub>R activation (Hajnóczky and Thomas, 1994), although the detailed mechanisms are unresolved.

Comparison of receptor occupancy and functional responses reveals that only a tiny fraction of a cell's IP<sub>3</sub>Rs contribute to incremental responses. These analyses, supported by simulations (Figures 7E–7T), reconcile incremental responses with IP<sub>3</sub>R inactivation. A surge of coordinated opening of IP<sub>3</sub>Rs occurs with each step in IP<sub>3</sub> concentration. This is followed by IP<sub>3</sub>R inactivation. Thereafter, there will never be the same balance in favor of the open state until the next step in IP<sub>3</sub> concentration triggers another coordinated sequence of IP<sub>3</sub>R opening and then inactivation (Figures 7F and 7L). Pulsatile delivery of IP<sub>3</sub> to intact cells may be provided by changes in extracellular stimulus intensity or

by cycles of IP<sub>3</sub> production and degradation driven by feedback regulation of phospholipase C in the sustained presence of an extracellular stimulus (Bartlett et al., 2015; Dupont et al., 2011; Meyer and Stryer, 1988; Nash et al., 2001).

Our results suggest a mechanism for incremental responses to IP<sub>3</sub>, a phenomenon that has remained unresolved for more than 30 years. Unrestrained IP<sub>3</sub>Rs might evoke explosive responses through CICR. The mechanism we propose allows cells to evoke rapid Ca<sup>2+</sup> signals through IP<sub>3</sub>Rs that are graded with stimulus intensity (Figure 1P).

## Limitations of the study

Two essential features underpin our explanation for incremental responses to IP<sub>3</sub>: rapid inactivation of IP<sub>3</sub>Rs after their opening, and physiological responses mediated by a tiny fraction of available IP<sub>3</sub>Rs. We do not yet understand the molecular mechanisms underlying IP<sub>3</sub>R inactivation, and notably whether accessory proteins are required. Understanding these mechanisms would allow us to refine our simplified scheme, which presently includes an irreversible step that forbids transitions from the closed (C<sub>4</sub>) to inactivated (I<sub>4</sub>) state of IP<sub>3</sub>Rs. Hence, our simplified scheme is not a closed cycle, suggesting that it is coupled to an additional mechanism, perhaps reflecting the need for additional proteins to mediate inactivation. High-resolution optical microscopy reveals that low concentrations of IP<sub>3</sub> evoke small, highly localized Ca<sup>2+</sup> signals (“Ca<sup>2+</sup> puffs”) in intact cells neighbors (Smith and Parker, 2009; Thillaiappan et al., 2021). It is not yet clear how incremental responses to IP<sub>3</sub> relate to Ca<sup>2+</sup> puffs.

## STAR★METHODS

Detailed methods are provided in the online version of this paper and include the following:

- KEY RESOURCES TABLE
- RESOURCE AVAILABILITY
  - Lead contact
  - Materials availability
  - Data and code availability
- EXPERIMENTAL MODEL AND SUBJECT DETAILS
  - Cells
- METHOD DETAILS
  - Synthesis of **2**
  - Cell culture and transfections
  - Ca<sup>2+</sup> release by IP<sub>3</sub>Rs
  - Fluorescence microscopy
  - Single-cell analyses of Ca<sup>2+</sup> release
  - [<sup>3</sup>H]IP<sub>3</sub> binding
  - Nuclear patch-clamp recording from IP<sub>3</sub>Rs
  - Western blotting
- QUANTIFICATION AND STATISTICAL ANALYSES
  - Simulations
  - Analysis

## SUPPLEMENTAL INFORMATION

Supplemental information can be found online at <https://doi.org/10.1016/j.celrep.2021.109932>.

## ACKNOWLEDGMENTS

This work was supported by the Biotechnology and Biological Sciences Research Council (BB/P005330/1 to C.W.T.), the Medical Research Council (MR/T028378/1 to C.W.T. and A.M. Rossi), Fondation Philippe Wiener-Maurice Anspach (to G.D. and C.W.T.), Senior Investigator Awards from Wellcome to C.W.T. (101844) and B.V.L.P. (101010), and a Royal Society Fellowship to T.R. (UF110479). A.M. Rossi is a fellow of Queens' College, Cambridge. G.D. is a Research Director at the Belgian FRS-FNRS. We thank Abdelhamid Yousef (Cambridge) for contributing ideas relating to *erlin 2*.

## AUTHOR CONTRIBUTIONS

A.M. Rossi performed all biological experiments, except the single-channel recordings. T.R. performed single-channel recordings. A.M. Riley and B.V.L.P. developed and synthesized compound 2. G.D. implemented the mathematical models. C.W.T. and A.M. Rossi designed the study, analyzed and interpreted results, and, with input from the other authors, wrote the manuscript. All authors reviewed the final manuscript.

## DECLARATION OF INTERESTS

The authors declare no competing interests.

Received: February 4, 2021

Revised: July 16, 2021

Accepted: October 12, 2021

Published: November 2, 2021

## REFERENCES

Alzayady, K.J., Seb  Pedr  s, A., Chandrasekhar, R., Wang, L., Ruiz-Trillo, I., and Yule, D.I. (2015). Tracing the evolutionary history of inositol, 1,4,5-trisphosphate receptor: Insights from analyses of *Capsaspora owczarzaki* Ca<sup>2+</sup> release channel orthologs. *Mol. Biol. Evol.* 32, 2236–2253.

Alzayady, K.J., Wang, L., Chandrasekhar, R., Wagner, L.E., 2nd, Van Petegem, F., and Yule, D.I. (2016). Defining the stoichiometry of inositol 1,4,5-trisphosphate binding required to initiate Ca<sup>2+</sup> release. *Sci. Signal.* 9, ra35.

Ames, B.N., and Dubin, D.T. (1960). The role of polyamines in the neutralization of bacteriophage deoxyribonucleic acid. *J. Biol. Chem.* 235, 769–775.

Arunlakshana, O., and Schild, H.O. (1959). Some quantitative uses of drug antagonists. *Br. J. Pharmacol. Chemother.* 14, 48–58.

Barrero, M.J., Montero, M., and Alvarez, J. (1997). Dynamics of [Ca<sup>2+</sup>] in the endoplasmic reticulum and cytoplasm of intact HeLa cells. A comparative study. *J. Biol. Chem.* 272, 27694–27699.

Bartlett, P.J., Metzger, W., Gaspers, L.D., and Thomas, A.P. (2015). Differential regulation of multiple steps in inositol 1,4,5-trisphosphate signaling by protein kinase C shapes hormone-stimulated Ca<sup>2+</sup> oscillations. *J. Biol. Chem.* 290, 18519–18533.

Beecroft, M.D., and Taylor, C.W. (1997). Incremental Ca<sup>2+</sup> mobilization by inositol trisphosphate receptors is unlikely to be mediated by their desensitization or regulation by luminal or cytosolic Ca<sup>2+</sup>. *Biochem. J.* 326, 215–220.

Berridge, M.J. (2016). The inositol trisphosphate/calcium signaling pathway in health and disease. *Physiol. Rev.* 96, 1261–1296.

Bezprozvanny, I., and Ehrlich, B.E. (1994). Inositol (1,4,5)-trisphosphate (InsP<sub>3</sub>)-gated Ca channels from cerebellum: Conduction properties for divalent cations and regulation by intraluminal calcium. *J. Gen. Physiol.* 104, 821–856.

Blagbrough, I.S., and Geall, A.J. (1998). Practical synthesis of unsymmetrical polyamine amides. *Tetrahedron Lett.* 39, 439–442.

Bootman, M. (1994). Intracellular calcium. Questions about quantal Ca<sup>2+</sup> release. *Curr. Biol.* 4, 169–172.

Bootman, M.D., Berridge, M.J., and Taylor, C.W. (1992). All-or-nothing Ca<sup>2+</sup> mobilization from the intracellular stores of single histamine-stimulated HeLa cells. *J. Physiol.* 450, 163–178.

Bosanac, I., Alattia, J.-R., Mal, T.K., Chan, J., Talarico, S., Tong, F.K., Tong, K.I., Yoshikawa, F., Furuichi, T., Iwai, M., et al. (2002). Structure of the inositol 1,4,5-trisphosphate receptor binding core in complex with its ligand. *Nature* 420, 696–700.

Callamaras, N., and Parker, I. (2000). Phasic characteristic of elementary Ca<sup>2+</sup> release sites underlies quantal responses to IP<sub>3</sub>. *EMBO J.* 19, 3608–3617.

Cheek, T.R., Berridge, M.J., Moreton, R.B., Stauderman, K.A., Murawsky, M.M., and Bootman, M.D. (1994). Quantal Ca<sup>2+</sup> mobilization by ryanodine receptors is due to all-or-none release from functionally discrete intracellular stores. *Biochem. J.* 301, 879–883.

Combettes, L., Claret, M., and Champeil, P. (1992). Do submaximal InsP<sub>3</sub> concentrations only induce the partial discharge of permeabilized hepatocyte calcium pools because of the concomitant reduction of intraluminal Ca<sup>2+</sup> concentration? *FEBS Lett.* 301, 287–290.

Dawson, A.P., Lea, E.J., and Irvine, R.F. (2003). Kinetic model of the inositol trisphosphate receptor that shows both steady-state and quantal patterns of Ca<sup>2+</sup> release from intracellular stores. *Biochem. J.* 370, 621–629.

Ding, Z., Rossi, A.M., Riley, A.M., Rahman, T., Potter, B.V.L., and Taylor, C.W. (2010). Binding of inositol 1,4,5-trisphosphate (IP<sub>3</sub>) and adenophostin A to the N-terminal region of the IP<sub>3</sub> receptor: Thermodynamic analysis using fluorescence polarization with a novel IP<sub>3</sub> receptor ligand. *Mol. Pharmacol.* 77, 995–1004.

Dohle, W., Su, X., Mills, S.J., Rossi, A.M., Taylor, C.W., and Potter, B.V.L. (2019). A synthetic cyclitol-nucleoside conjugate polyphosphate is a highly potent second messenger mimic. *Chem. Sci. (Camb.)* 10, 5382–5390.

Dupont, G., Combettes, L., Bird, G.S., and Putney, J.W. (2011). Calcium oscillations. *Cold Spring Harb. Perspect. Biol.* 3, a004226.

Ferrell, J.E., Jr. (2016). Perfect and near-perfect adaptation in cell signaling. *Cell Syst.* 2, 62–67.

Ferris, C.D., Cameron, A.M., Haganir, R.L., and Snyder, S.H. (1992). Quantal calcium release by purified reconstituted inositol 1,4,5-trisphosphate receptors. *Nature* 356, 350–352.

Hajn  czky, G., and Thomas, A.P. (1994). The inositol trisphosphate calcium channel is inactivated by inositol trisphosphate. *Nature* 370, 474–477.

Hajn  czky, G., Lin, C., and Thomas, A.P. (1994). Luminal communication between intracellular calcium stores modulated by GTP and the cytoskeleton. *J. Biol. Chem.* 269, 10280–10287.

Hannaert-Merah, Z., Coquil, J.-F., Combettes, L., Claret, M., Mauger, J.-P., and Champeil, P. (1994). Rapid kinetics of myo-inositol trisphosphate binding and dissociation in cerebellar microsomes. *J. Biol. Chem.* 269, 29642–29649.

Hill, T.D., Dean, N.M., and Boynton, A.L. (1988). Inositol 1,3,4,5-tetrakisphosphate induces Ca<sup>2+</sup> sequestration in rat liver cells. *Science* 242, 1176–1178.

Hirose, K., and Iino, M. (1994). Heterogeneity of channel density in inositol-1,4,5-trisphosphate-sensitive Ca<sup>2+</sup> stores. *Nature* 372, 791–794.

Ionescu, L., Cheung, K.H., Vais, H., Mak, D.O., White, C., and Foskett, J.K. (2006). Graded recruitment and inactivation of single InsP<sub>3</sub> receptor Ca<sup>2+</sup>-release channels: implications for quantal [corrected] Ca<sup>2+</sup> release. *J. Physiol.* 573, 645–662.

Irvine, R.F. (1990). “Quantal” Ca<sup>2+</sup> release and the control of Ca<sup>2+</sup> entry by inositol phosphates—A possible mechanism. *FEBS Lett.* 263, 5–9.

Iwai, M., Tateishi, Y., Hattori, M., Mizutani, A., Nakamura, T., Futatsugi, A., Inoue, T., Furuichi, T., Michikawa, T., and Mikoshiba, K. (2005). Molecular cloning of mouse type 2 and type 3 inositol 1,4,5-trisphosphate receptors and identification of a novel type 2 receptor splice variant. *J. Biol. Chem.* 280, 10305–10317.

Lampe, D., Liu, C., and Potter, B.V.L. (1994). Synthesis of selective non-Ca<sup>2+</sup>-mobilizing inhibitors of D-myo-inositol 1,4,5-trisphosphate 5-phosphatase. *J. Med. Chem.* 37, 907–912.

Lytton, J., Westlin, M., Burk, S.E., Shull, G.E., and MacLennan, D.H. (1992). Functional comparisons between isoforms of the sarcoplasmic or endoplasmic reticulum family of calcium pumps. *J. Biol. Chem.* 267, 14483–14489.



- Mak, D.-O., and Foskett, J.K. (1997). Single-channel kinetics, inactivation, and spatial distribution of inositol trisphosphate (IP<sub>3</sub>) receptors in *Xenopus* oocyte nucleus. *J. Gen. Physiol.* 109, 571–587.
- Mak, D.-O., McBride, S., Raghuram, V., Yue, Y., Joseph, S.K., and Foskett, J.K. (2000). Single-channel properties in endoplasmic reticulum membrane of recombinant type 3 inositol trisphosphate receptor. *J. Gen. Physiol.* 115, 241–256.
- Mak, D.-O., McBride, S., and Foskett, J.K. (2001). Regulation by Ca<sup>2+</sup> and inositol 1,4,5-trisphosphate (InsP<sub>3</sub>) of single recombinant type 3 InsP<sub>3</sub> receptor channels. Ca<sup>2+</sup> activation uniquely distinguishes types 1 and 3 insp3 receptors. *J. Gen. Physiol.* 117, 435–446.
- Marchant, J.S., and Taylor, C.W. (1997). Cooperative activation of IP<sub>3</sub> receptors by sequential binding of IP<sub>3</sub> and Ca<sup>2+</sup> safeguards against spontaneous activity. *Curr. Biol.* 7, 510–518.
- Marchant, J.S., and Taylor, C.W. (1998). Rapid activation and partial inactivation of inositol trisphosphate receptors by inositol trisphosphate. *Biochemistry* 37, 11524–11533.
- Marshall, I.C.B., and Taylor, C.W. (1994). Two calcium-binding sites mediate the interconversion of liver inositol 1,4,5-trisphosphate receptors between three conformational states. *Biochem. J.* 301, 591–598.
- Mataragka, S., and Taylor, C.W. (2018). All three IP<sub>3</sub> receptor subtypes generate Ca<sup>2+</sup> puffs, the universal building blocks of IP<sub>3</sub>-evoked Ca<sup>2+</sup> signals. *J. Cell Sci.* 131, jcs220848.
- Meyer, T., and Stryer, L. (1988). Molecular model for receptor-stimulated calcium spiking. *Proc. Natl. Acad. Sci. USA* 85, 5051–5055.
- Meyer, T., and Stryer, L. (1990). Transient calcium release induced by successive increments of inositol 1,4,5-trisphosphate. *Proc. Natl. Acad. Sci. USA* 87, 3841–3845.
- Missiaen, L., De Smedt, H., Droogmans, G., and Casteels, R. (1992). Ca<sup>2+</sup> release induced by inositol 1,4,5-trisphosphate is a steady-state phenomenon controlled by luminal Ca<sup>2+</sup> in permeabilized cells. *Nature* 357, 599–602.
- Muallem, S., Pandol, S.J., and Beeker, T.G. (1989). Hormone-evoked calcium release from intracellular stores is a quantal process. *J. Biol. Chem.* 264, 205–212.
- Nash, M.S., Young, K.W., Challiss, R.A.J., and Nahorski, S.R. (2001). Intracellular signalling. Receptor-specific messenger oscillations. *Nature* 413, 381–382.
- Oldershaw, K.A., Nunn, D.L., and Taylor, C.W. (1991). Quantal Ca<sup>2+</sup> mobilization stimulated by inositol 1,4,5-trisphosphate in permeabilized hepatocytes. *Biochem. J.* 278, 705–708.
- Oldershaw, K.A., Richardson, A., and Taylor, C.W. (1992). Prolonged exposure to inositol 1,4,5-trisphosphate does not cause intrinsic desensitization of the intracellular Ca<sup>2+</sup>-mobilizing receptor. *J. Biol. Chem.* 267, 16312–16316.
- Pantazaka, E., and Taylor, C.W. (2011). Differential distribution, clustering, and lateral diffusion of subtypes of the inositol 1,4,5-trisphosphate receptor. *J. Biol. Chem.* 286, 23378–23387.
- Parker, I., and Ivorra, I. (1990). Localized all-or-none calcium liberation by inositol trisphosphate. *Science* 250, 977–979.
- Parys, J.B., Missiaen, L., De Smedt, H., and Casteels, R. (1993). Loading dependence of inositol 1,4,5-trisphosphate-induced Ca<sup>2+</sup> release in the clonal cell line A7r5. Implications for the mechanism of quantal Ca<sup>2+</sup> release. *J. Biol. Chem.* 268, 25206–25212.
- Prins, D., and Michalak, M. (2011). Organellar calcium buffers. *Cold Spring Harb. Perspect. Biol.* 3, 004069.
- Qin, F. (2004). Restoration of single-channel currents using the segmental k-means method based on hidden Markov modeling. *Biophys. J.* 86, 1488–1501.
- Renard-Rooney, D.C., Hajnóczky, G., Seitz, M.B., Schneider, T.G., and Thomas, A.P. (1993). Imaging of inositol 1,4,5-trisphosphate-induced Ca<sup>2+</sup> fluxes in single permeabilized hepatocytes. Demonstration of both quantal and nonquantal patterns of Ca<sup>2+</sup> release. *J. Biol. Chem.* 268, 23601–23610.
- Richardson, A., and Taylor, C.W. (1993). Effects of Ca<sup>2+</sup> chelators on purified inositol 1,4,5-trisphosphate (InsP<sub>3</sub>) receptors and InsP<sub>3</sub>-stimulated Ca<sup>2+</sup> mobilization. *J. Biol. Chem.* 268, 11528–11533.
- Riley, A.M., Dozol, H., Spiess, B., and Potter, B.V.L. (2004). 2-O-(2-aminoethyl)-myo-inositol 1,4,5-trisphosphate as a novel ligand for conjugation: physicochemical properties and synthesis of a new Ins(1,4,5)P<sub>3</sub> affinity matrix. *Biochem. Biophys. Res. Commun.* 318, 444–452.
- Ríos, E. (2018). Calcium-induced release of calcium in muscle: 50 years of work and the emerging consensus. *J. Gen. Physiol.* 150, 521–537.
- Rossi, A.M., and Taylor, C.W. (2020). Reliable measurement of free Ca<sup>2+</sup> concentrations in the ER lumen using Mag-Fluo-4. *Cell Calcium* 87, 102188.
- Rossi, A.M., Riley, A.M., Tovey, S.C., Rahman, T., Dellis, O., Taylor, E.J.A., Veresov, V.G., Potter, B.V.L., and Taylor, C.W. (2009). Synthetic partial agonists reveal key steps in IP<sub>3</sub> receptor activation. *Nat. Chem. Biol.* 5, 631–639.
- Saleem, H., Tovey, S.C., Molinski, T.F., and Taylor, C.W. (2014). Interactions of antagonists with subtypes of inositol 1,4,5-trisphosphate (IP<sub>3</sub>) receptor. *Br. J. Pharmacol.* 171, 3298–3312.
- Schindelin, J., Arganda-Carreras, I., Frise, E., Kaynig, V., Longair, M., Pietzsch, T., Preibisch, S., Rueden, C., Saalfeld, S., Schmid, B., et al. (2012). Fiji: An open-source platform for biological-image analysis. *Nat. Methods* 9, 676–682.
- Shaw, G., Morse, S., Ararat, M., and Graham, F.L. (2002). Preferential transformation of human neuronal cells by human adenoviruses and the origin of HEK 293 cells. *FASEB J.* 16, 869–871.
- Shen, D., Wang, X., Li, X., Zhang, X., Yao, Z., Dibble, S., Dong, X.P., Yu, T., Lieberman, A.P., Showalter, H.D., and Xu, H. (2012). Lipid storage disorders block lysosomal trafficking by inhibiting a TRP channel and lysosomal calcium release. *Nat. Commun.* 3, 731.
- Shuttleworth, T.J. (1992). Ca<sup>2+</sup> release from inositol trisphosphate-sensitive stores is not modulated by intraluminal [Ca<sup>2+</sup>]. *J. Biol. Chem.* 267, 3573–3576.
- Smith, I.F., and Parker, I. (2009). Imaging the quantal substructure of single IP<sub>3</sub>R channel activity during Ca<sup>2+</sup> puffs in intact mammalian cells. *Proc. Natl. Acad. Sci. USA* 106, 6404–6409.
- Stehno-Bittel, L., Lückhoff, A., and Clapham, D.E. (1995). Calcium release from the nucleus by InsP<sub>3</sub> receptor channels. *Neuron* 14, 163–167.
- Stephenson, R.P. (1956). A modification of receptor theory. *Br. J. Pharmacol. Chemother.* 11, 379–393.
- Subramanian, K., and Meyer, T. (1997). Calcium-induced restructuring of nuclear envelope and endoplasmic reticulum calcium stores. *Cell* 89, 963–971.
- Sugawara, H., Kurosaki, M., Takata, M., and Kurosaki, T. (1997). Genetic evidence for involvement of type 1, type 2 and type 3 inositol 1,4,5-trisphosphate receptors in signal transduction through the B-cell antigen receptor. *EMBO J.* 16, 3078–3088.
- Supattapone, S., Worley, P.F., Baraban, J.M., and Snyder, S.H. (1988). Solubilization, purification, and characterization of an inositol trisphosphate receptor. *J. Biol. Chem.* 263, 1530–1534.
- Suzuki, J., Kanemaru, K., Ishii, K., Ohkura, M., Okubo, Y., and Iino, M. (2014). Imaging intraorganellar Ca<sup>2+</sup> at subcellular resolution using CEPIA. *Nat. Commun.* 5, 4153.
- Suzuki, J., Kanemaru, K., and Iino, M. (2016). Genetically encoded fluorescent indicators for organellar calcium imaging. *Biophys. J.* 111, 1119–1131.
- Taufiq-Ur-Rahman, Skupin, A., Falcke, M., and Taylor, C.W. (2009). Clustering of InsP<sub>3</sub> receptors by InsP<sub>3</sub> retunes their regulation by InsP<sub>3</sub> and Ca<sup>2+</sup>. *Nature* 458, 655–659.
- Taylor, C.W., and Potter, B.V.L. (1990). The size of inositol 1,4,5-trisphosphate-sensitive Ca<sup>2+</sup> stores depends on inositol 1,4,5-trisphosphate concentration. *Biochem. J.* 266, 189–194.
- Thillaiappan, N.B., Chavda, A.P., Tovey, S.C., Prole, D.L., and Taylor, C.W. (2017). Ca<sup>2+</sup> signals initiate at immobile IP<sub>3</sub> receptors adjacent to ER-plasma membrane junctions. *Nat. Commun.* 8, 1505.
- Thillaiappan, N.B., Smith, H.A., Atakpa-Adaji, P., and Taylor, C.W. (2021). KRAP tethers IP<sub>3</sub> receptors to actin and licenses them to evoke cytosolic Ca<sup>2+</sup> signals. *Nat. Commun.* 12, 4514.



- Tovey, S.C., Sun, Y., and Taylor, C.W. (2006). Rapid functional assays of intracellular  $\text{Ca}^{2+}$  channels. *Nat. Protoc.* 1, 259–263.
- Tregear, R.T., Dawson, A.P., and Irvine, R.F. (1991). Quantal release of  $\text{Ca}^{2+}$  from intracellular stores by  $\text{InsP}_3$ : tests of the concept of control of  $\text{Ca}^{2+}$  release by intraluminal  $\text{Ca}^{2+}$ . *Proc. Biol. Sci.* 243, 263–268.
- Tveito, A., and Lines, G.T. (2010). Computing Characterizations of Drugs for Ion Channels and Receptors Using Markov Models (SpringerOpen).
- Vais, H., Foskett, J.K., and Mak, D.O. (2010). Unitary  $\text{Ca}^{2+}$  current through recombinant type 3  $\text{InsP}_3$  receptor channels under physiological ionic conditions. *J. Gen. Physiol.* 136, 687–700.
- Vais, H., Foskett, J.K., Ullah, G., Pearson, J.E., and Mak, D.O. (2012). Permeant calcium ion feed-through regulation of single inositol 1,4,5-trisphosphate receptor channel gating. *J. Gen. Physiol.* 140, 697–716.
- Vais, H., Wang, M., Mallilankaraman, K., Payne, R., McKennan, C., Lock, J.T., Spruce, L.A., Fiest, C., Chan, M.Y., Parker, I., et al. (2020). ER-luminal  $[\text{Ca}^{2+}]$  regulation of  $\text{InsP}_3$  receptor gating mediated by an ER-luminal peripheral  $\text{Ca}^{2+}$ -binding protein. *eLife* 9, e53531.
- Valm, A.M., Cohen, S., Legant, W.R., Melunis, J., Hershberg, U., Wait, E., Cohen, A.R., Davidson, M.W., Betzig, E., and Lippincott-Schwartz, J. (2017). Applying systems-level spectral imaging and analysis to reveal the organelle interactome. *Nature* 546, 162–167.
- Venkatachalam, K., Hofmann, T., and Montell, C. (2006). Lysosomal localization of TRPML3 depends on TRPML2 and the mucopolipidosis-associated protein TRPML1. *J. Biol. Chem.* 281, 17517–17527.
- Wang, S.Q., Stern, M.D., Ríos, E., and Cheng, H. (2004). The quantal nature of  $\text{Ca}^{2+}$  sparks and in situ operation of the ryanodine receptor array in cardiac cells. *Proc. Natl. Acad. Sci. USA* 101, 3979–3984.
- Wiltgen, S.M., Dickinson, G.D., Swaminathan, D., and Parker, I. (2014). Termination of calcium puffs and coupled closings of inositol trisphosphate receptor channels. *Cell Calcium* 56, 157–168.
- Winding, P., and Berchtold, M.W. (2001). The chicken B cell line DT40: A novel tool for gene disruption experiments. *J. Immunol. Methods* 249, 1–16.
- Wojcikiewicz, R.J.H. (1995). Type I, II, and III inositol 1,4,5-trisphosphate receptors are unequally susceptible to down-regulation and are expressed in markedly different proportions in different cell types. *J. Biol. Chem.* 270, 11678–11683.
- Wojcikiewicz, R.J.H. (2018). The making and breaking of inositol 1,4,5-trisphosphate receptor tetramers. *Messenger (Los Angel.)* 6, 45–49.
- Yamashita, M. (2006). “Quantal”  $\text{Ca}^{2+}$  release reassessed—A clue to oscillation and synchronization. *FEBS Lett.* 580, 4979–4983.
- Yamashita, M., Sugioka, M., and Ogawa, Y. (2006). Voltage- and  $\text{Ca}^{2+}$ -activated potassium channels in  $\text{Ca}^{2+}$  store control  $\text{Ca}^{2+}$  release. *FEBS J.* 273, 3585–3597.
- Yoshikawa, F., Iwasaki, H., Michikawa, T., Furuichi, T., and Mikoshiba, K. (1999). Cooperative formation of the ligand-binding site of the inositol 1,4,5-trisphosphate receptor by two separable domains. *J. Biol. Chem.* 274, 328–334.

## STAR★METHODS

### KEY RESOURCES TABLE

REAGENT or RESOURCE	SOURCE	IDENTIFIER
<b>Antibodies</b>		
Anti-IP <sub>3</sub> R Ab (AbC, recognizes all vertebrate IP <sub>3</sub> R subtypes, rabbit, monoclonal) (1:1000)	Cell Signaling Technology (Danvers, MA, USA)	Cat#8568S Clone # D53A5 RRID: AB_10890699
Anti-β-actin Ab (mouse monoclonal) (1:30000)	Cell Signaling Technology	Cat#3700S Clone # 8H10D10 RRID: AB_2242334
Anti-erlin 2 Ab (rabbit, monoclonal) (1:1000)	Abcam (Cambridge, UK)	Cat#ab129207 Clone # EPR8088 RRID:AB_11143745
Anti-mouse secondary Ab (mouse IgG κ-binding protein conjugated to horseradish peroxidase, HRP) (1:5000)	Santa Cruz (Dallas, TX, USA)	Cat#sc-516102 RRID: AB_2687626
Anti-rabbit secondary Ab (goat monoclonal, conjugated to HRP) (1:5000)	SeraCare (Milford, MA, USA)	Cat#5220-0336 RRID: AB_2857917
<b>Chemicals, peptides, and recombinant proteins</b>		
2-aminoethoxy diphenyl borate (2-APB)	BioVision (Milpitas, CA, USA)	Cat#1798-100
ATP	Sigma-Aldrich (St. Louis, MO, USA)	Cat#A6419
Bafilomycin A <sub>1</sub>	Fluorochem (Hadfield, UK).	Cat#M01404
BAPTA	Phion (Dorset, UK)	Cat#61061782
Bis(4-nitrophenyl) carbonate	Acros Organics via ThermoFisher (Waltham, MA, USA)	Cat#171600250
Cbz <sub>3</sub> -spermine-IP <sub>3</sub> (2)	Synthesis and properties described in this paper	<a href="#">Figure 2A</a>
Chelex-100 resin Na <sup>+</sup> form	Sigma-Aldrich	Cat#C7901
Cyclopiazonic acid (CPA)	Tocris (Bristol, UK)	Cat#1235
Dequalinium chloride hydrate	Sigma-Aldrich	Cat#D3768
D-myo-inositol 1,4,5-trisphosphate (IP <sub>3</sub> )	Enzo (Exeter, UK)	Cat#ALX-307-007-M005
D-myo-[ <sup>3</sup> H]inositol 1,4,5-trisphosphate ([ <sup>3</sup> H] IP <sub>3</sub> ) (19.3-21 Ci/mmol)	PerkinElmer (Beaconsfield, UK)	Cat#NET911005UC
D-myo-inositol 2,4,5-trisphosphate ((2,4,5)IP <sub>3</sub> )	Cayman Chemical (Ann Arbor, MI, USA)	Cat#10007779
Dulbecco's modified Eagle's medium/nutrient mixture F-12 with GlutaMAX (DMEM/F-12 GlutaMAX)	ThermoFisher	<b>Cat#10565018</b>
Foetal bovine serum (FBS)	Sigma	Cat#F7524
G418	Formedium (Norfolk, UK)	Cat#G4181
Heparin, sodium salt	Calbiochem via Merck (Watford, UK)	Cat#375095
Ionomycin, Ca <sup>2+</sup> salt	Apollo Scientific (Stockport, UK)	Cat#BII0123
LiChroprep RP-18 (25-40 μm)	Merck	Cat#109303
Mag-fluo 4 AM	ThermoFisher	Cat#M14206
ML-SA1	Merck	Cat#648493
Poly-L-lysine (1% solution)	Sigma	Cat#P8920
Q-Sepharose Fast Flow resin	GE Healthcare (Chicago, IL, USA)	Cat#GE17-0510-01
Saponin	Sigma-Aldrich	Cat#S4521

(Continued on next page)

**Continued**

REAGENT or RESOURCE	SOURCE	IDENTIFIER
Thapsigargin	Bio-Techne (Middlesex, UK)	Cat#1138/1
Triethylamine	Sigma-Aldrich	Cat#90340
<b>Critical commercial assays</b>		
8-well glass-bottom $\mu$ -slides	Ibidi (Munich, Germany)	Cat#80827
35-mm glass bottom dishes (#1 glass)	Cellvis (Mountain View, CA 94039)	Cat#D35-14-1-N
ECL-Prime/Select western blotting reagents	Amersham via GE Healthcare	Cat#RPN2236/RPN2235
Half-area 96-well black-walled plates	Greiner, Bio-One (Stonehouse, UK)	Cat#675090
Neon transfection system kit	ThermoFisher	Cat#MPK10096
iBlot gel-transfer stacks PVDF	ThermoFisher	Cat#IB401001
Protease inhibitor cocktail (Roche)	Merck	Cat#11836153001
NuPAGE, SDS-PAGE gels (3-8% Tris-acetate or 4-12% Bis-Tris)	ThermoFisher	Cat#EA0375BOX or NP0321BOX
TransIT-LT1 transfection reagent	Geneflow (Lichfield, UK)	Cat#MIR 2305
<b>Experimental models: Cell lines</b>		
<i>Gallus gallus</i> DT40-IP <sub>3</sub> R1 (DT40-IP <sub>3</sub> R2; DT40-IP <sub>3</sub> R3) cells	<a href="#">Tovey et al., 2006</a>	N/A
<i>Homo sapiens</i> HEK-3KO cells	Kerafast (Boston, MA, USA) ( <a href="#">Alzayady et al., 2016</a> )	Cat#EUR030
<i>Homo sapiens</i> HEK-G-CEPIAer cells	This paper	N/A
<i>Homo sapiens</i> wild-type HEK293 cells	Dr D Yule, University of Rochester, NY, USA	N/A
<b>Oligonucleotides</b>		
siRNA targeting sequence of Erlin 2 (siRNA 1) ATCTACTTTGACAGAATTGAA	QIAGEN (Manchester, UK)	Cat#SI04952689
siRNA targeting sequence of Erlin 2 (siRNA 2) AAGATAGAAGAGGGACATATT	QIAGEN	Cat#SI04952696
Non-silencing (NS) siRNA	QIAGEN	Cat#1027280
<b>Recombinant DNA</b>		
CFP-TRPML1 plasmid	Addgene ( <a href="#">Venkatachalam et al., 2006</a> )	Cat#18827
G-CEPIA1er plasmid	Addgene ( <a href="#">Suzuki et al., 2016</a> )	Cat#58215
IP <sub>3</sub> R1 in pcDNA3.1(-)/Myc-His B plasmid	<a href="#">Dohle et al., 2019</a>	N/A
EGFP-IP <sub>3</sub> R1 in pcDNA3.2/DEST	<a href="#">Pantazaka and Taylor, 2011</a>	N/A
Residues 1-604 of rat IP <sub>3</sub> R1 (NT) in pTrcHisA plasmid	<a href="#">Rossi et al., 2009</a>	N/A
Residues 224-604 of rat IP <sub>3</sub> R1 (IBC) in pTrcHisA plasmid	<a href="#">Rossi et al., 2009</a>	N/A
<b>Software and algorithms</b>		
Fiji		<a href="#">Schindelin et al., 2012</a>
MetaMorph. Version 7.10.1.161	Molecular Devices (San Jose, CA, USA)	N/A
PRISM. Version 8.4.2	GraphPad Software (La Jolla, CA, USA)	N/A
QuB	<a href="#">Qin, 2004</a>	N/A
SoftMax Pro. Version 5.4	Molecular Devices	N/A
Codes for simulations	This paper	Available from: <a href="https://github.com/genedupont/Quantal">https://github.com/genedupont/Quantal</a>

**RESOURCE AVAILABILITY**

**Lead contact**

Requests for resources and reagents should be directed to the Lead Contact, Colin W. Taylor ([cwt1000@cam.ac.uk](mailto:cwt1000@cam.ac.uk)).

### Materials availability

All plasmids used are commercially available, except EGFP-IP<sub>3</sub>R1 which is available from the Lead Contact. The cell lines generated in this study are available from the Lead Contact. Compound **2** is available from Barry V. L. Potter (barry.potter@pharm.ox.ac.uk).

### Data and code availability

No large datasets were generated by this study. The computer code used for the simulations is available at: <https://github.com/genedupont/Quantal>. Any additional information required to reanalyze the data reported in this paper is available from the lead contact upon request.

## EXPERIMENTAL MODEL AND SUBJECT DETAILS

### Cells

DT40 cells are an avian B cell line, wherein high rates of DNA recombination have been widely exploited for analyses of cell signaling and B cell function (Winding and Berchtold, 2001). DT40 cells were the first cells in which all three IP<sub>3</sub>R subtypes were genetically disrupted to provide a null-background for IP<sub>3</sub>R expression (Sugawara et al., 1997). We used DT40 cells without native IP<sub>3</sub>R to generate cell lines stably expressing single subtypes of mammalian IP<sub>3</sub>R (DT40-IP<sub>3</sub>R1-3) (Tovey et al., 2006).

Human embryonic kidney 293 (HEK293 cells) are hypotriploid cells derived from embryonic kidney and immortalized by transfection with adenovirus (Shaw et al., 2002). We used wild-type HEK cells (which express all three IP<sub>3</sub>R subtypes) (Mataragka and Taylor, 2018), and a stable cell line in which CRISPR/Cas9 was used to prevent expression of all native IP<sub>3</sub>R (HEK-3KO) (Alzayady et al., 2016). HEK-3KO cells were transfected with mammalian IP<sub>3</sub>R1 to generate a monoclonal HEK-IP<sub>3</sub>R1 cell line, and wild-type HEK cells were used to generate HEK-G-CEPIA1er cells stably expressing the ER-targeted genetically-encoded Ca<sup>2+</sup> indicator, G-CEPIA1er.

The identity of the parental HEK293 cell line used to generate HEK-3KO cells was confirmed by genotyping (Alzayady et al., 2016), and we confirmed the absence of all IP<sub>3</sub>R by western blotting (Mataragka and Taylor, 2018). None of the other cell lines was authenticated. All cells were periodically (every 2 months) confirmed to be free of mycoplasma.

## METHOD DETAILS

### Synthesis of **2**

We originally synthesized **2** (2-O-(1,5,10-tris(benzyloxycarbonyl)-15-oxo-1,5,10,14,16-pentaazaoctadecan-18-yl)-1D-*myo*-inositol 1,4,5-trisphosphate, Figure 2A) as an intermediate in the synthesis of a novel polyamine-IP<sub>3</sub> conjugate, but **2** proved to be most useful for our present purposes. Bis(4-nitrophenyl) carbonate was recrystallized from CH<sub>2</sub>Cl<sub>2</sub>/hexane. D-2-O-(2-aminoethyl)-IP<sub>3</sub> was synthesized as previously reported (Riley et al., 2004) and used as the triethylammonium salt. N<sup>1</sup>,N<sup>5</sup>,N<sup>10</sup>-tri(benzyloxycarbonyl)spermine was synthesized according to (Blagbrough and Geall, 1998). Triethylammonium bicarbonate (TEAB) buffer was made by bubbling CO<sub>2</sub> through a chilled aqueous solution of triethylamine. Anion-exchange chromatography was carried out on Q-Sepharose Fast Flow resin (GE Healthcare) using a Pharmacia Biotech GradiFrac system and P-1 pump, eluting at 5 mL/min with a linear gradient (0 to 100%) of 2.0 M aqueous TEAB buffer, collecting 10-mL fractions. Phosphate-containing fractions were identified using a modification of the Briggs phosphate test (Lampe et al., 1994). Reverse-phase ion-pair chromatography was carried out on LiChroprep RP-18 (25–40 μm, Merck) using a BioLogic LP system (BioRad), eluting at 5 mL/min with a linear gradient (0 to 70%) of CH<sub>3</sub>CN in 0.05 M TEAB buffer, collecting 7-mL fractions. Compound **2** was accurately quantified using the Ames phosphate assay (Ames and Dubin, 1960). All water used was MilliQ quality.

To a solution of bis(4-nitrophenyl) carbonate (200 mg, 0.66 mmol) in dry CH<sub>2</sub>Cl<sub>2</sub> (5 mL) under N<sub>2</sub> was added a solution of N<sup>1</sup>,N<sup>5</sup>,N<sup>10</sup>-tri(benzyloxycarbonyl)spermine (400 mg, 0.66 mmol) in dry CH<sub>2</sub>Cl<sub>2</sub>, dropwise over 10 min. The solution was stirred for 1 hr, after which TLC (CH<sub>2</sub>Cl<sub>2</sub>/MeOH 10:1 v/v) showed that all the amine (streak, R<sub>f</sub> 0.06) had been consumed, with appearance of a product at R<sub>f</sub> 0.72 (yellow on heating and stains with phosphomolybdic acid), together with 4-nitrophenol (R<sub>f</sub> 0.5) and a trace of unreacted bis(4-nitrophenyl) carbonate (R<sub>f</sub> 0.86). CH<sub>2</sub>Cl<sub>2</sub> (20 mL) was added, and the solution was washed with saturated aqueous NaHCO<sub>3</sub> (3 × 20 mL). The pale yellow organic layer was dried (MgSO<sub>4</sub>) and concentrated to give a yellow oil, which was purified by flash chromatography (CH<sub>2</sub>Cl<sub>2</sub>, then CH<sub>2</sub>Cl<sub>2</sub>:MeOH, 50:1 v/v) to give 4-nitrophenyl *N*-alkylcarbamate (436 mg) as a colorless oil; TLC R<sub>f</sub> 0.24 (CH<sub>2</sub>Cl<sub>2</sub>/EtOAc, 5:1). A solution of this alkylcarbamate (46 mg, 60 μmol) in CD<sub>3</sub>OD (0.75 mL) was added to solid D-2-O-(2-aminoethyl)-IP<sub>3</sub> (triethylammonium salt, 21 mg, 28 μmol) under N<sub>2</sub> in a 5-mL round-bottom flask, followed by dry triethylamine (40 μL). A deep yellow color (4-nitrophenol) appeared within seconds. The clear yellow solution was stirred at room temperature for 2 hr, then transferred to an NMR tube. The <sup>31</sup>P NMR spectrum of this solution showed three major peaks (1.01, 3.17 and 4.18 ppm) corresponding to **2**, together with other, smaller peaks. The solution was left for 16 hr in the NMR tube, after which a second <sup>31</sup>P NMR spectrum showed only the three product peaks. The reaction was therefore judged to be complete. The contents of the NMR tube were transferred to a 100-mL round-bottom flask and the NMR tube was rinsed with MeOH (1 mL). To the combined washings was added triethylammonium bicarbonate (TEAB) buffer (0.05 M, pH 7.6, 75 mL), and the resulting cloudy yellow solution was left for 16 hr at room temperature to hydrolyse any unreacted *N*-alkylcarbamate. The solution was then loaded onto a column of Q-Sepharose Fast Flow resin (120 mm × 16 mm, bicarbonate form). The column was washed well with

water (200 mL) and then eluted with a gradient of TEAB (2.0 M, 0 to 100%). At approx. 40% 2.0 M TEAB, the column eluent took on an intense yellow color (4-nitrophenol) and this buffer concentration was held constant until the eluent became colorless. When the concentration of TEAB was then allowed to increase, the target compound eluted above 90% 2.0 M TEAB. Fractions containing the target compound were identified using the Briggs phosphate assay, combined and concentrated under reduced pressure to give a colorless glassy residue (40 mg).  $^1\text{H}$  NMR spectroscopy of the product at this stage showed that it contained significant amounts of alkylammonium contaminants, resulting from the high concentration of TEAB buffer needed to elute it from the column. It was therefore purified further using reverse-phase ion-pair chromatography: the 40 mg of material was taken up in 0.05 M TEAB (5 mL) and loaded onto a column of LiChroprep RP-18 resin (100 mm  $\times$  16 mm). The column was washed well with 0.05 M TEAB, and then eluted with a gradient of  $\text{CH}_3\text{CN}$  in 0.05 M TEAB (0 to 70%  $\text{CH}_3\text{CN}$ ). The target eluted at 33%–40%  $\text{CH}_3\text{CN}$ , as detected by UV absorption at 254 nm. Fractions containing the target compound were combined and concentrated under reduced pressure. MeOH was repeatedly added and evaporated until a colorless glass remained ( $\sim$ 35 mg). Finally, this material was dissolved in water (5 mL) and passed through a column of Chelex-100 resin ( $\text{Na}^+$  form, 70 mm deep in a Pasteur pipette) to remove triethylammonium ions. The column was washed with water (5 mL) and the combined eluents were lyophilised to give **2** as a white, fluffy solid (28 mg, 19.7  $\mu\text{mol}$ , 70% as determined by total phosphate assay);  $^1\text{H}$  NMR ( $\text{Na}^+$  salt in  $\text{D}_2\text{O}$ , 400 MHz)  $\delta$  1.16–1.48 (4H, broad m, 2  $\times$  spermine  $\text{CH}_2$ ), 1.49–1.80 (4H, broad m, 2  $\times$  spermine  $\text{CH}_2$ ), 2.90–3.32 (12H, broad m, 6  $\times$  spermine  $\text{CH}_2$ ), 3.39 (2H, broad s,  $\text{NCH}_2\text{CH}_2\text{O}$ ), 3.80 (1H, broad d,  $J$  9.9 Hz, inositol H-3), 3.87–4.13 (5H, m, inositol H-1, H-5, H-6 and  $\text{NCH}_2\text{CH}_2\text{O}$ ), 4.15 (1H, broad s, inositol H-2), 4.33 (1H, q,  $J$  9.1 Hz, inositol H-4), 4.92–5.14 (6H, m, 3  $\times$   $\text{OCH}_2\text{Ph}$ ), 7.14–7.45 (15H, m, Ph);  $^{13}\text{C}$  NMR ( $\text{Na}^+$  salt in  $\text{D}_2\text{O}$ , 126 MHz)  $\delta$  24.42, 29.96, 27.35 and 28.02 (spermine  $\text{CH}_2$ ), 37.40 and 38.01 (spermine  $\text{CH}_2$ ), 40.20 ( $\text{NCH}_2\text{CH}_2\text{O}$ ), 44.04, 45.01 and 46.40 (spermine  $\text{CH}_2$ ), 66.51 and 67.20 (3  $\times$   $\text{OCH}_2\text{Ph}$ ), 71.38 (inositol C-3), 71.91 (inositol C-6), 72.72 ( $\text{NCH}_2\text{CH}_2\text{O}$ ), 74.59 (inositol C-1), 76.46 (inositol C-4), 78.31 (inositol C-5), 79.69 (inositol C-2), 127.53–128.58 (CH of Ph), 136.27 and 136.60 (*ipso*-C of Ph), 157.21, 157.37 and 157.82 (3  $\times$  urethane C = O), 160.56 (urea C = O);  $^{31}\text{P}$  NMR (triethylammonium salt in  $\text{CD}_3\text{OD}$ , 162 MHz,  $^1\text{H}$ -decoupled)  $\delta$  0.81 (1 P), 1.55 (1 P) and 2.50 (1 P); HRMS ( $m/z$ ) [ $\text{M}-\text{H}$ ] $^-$  calcd for  $\text{C}_{43}\text{H}_{62}\text{N}_5\text{O}_{22}\text{P}_3$ , 1092.3027; found 1092.3017.

### Cell culture and transfections

Methods used to generate and culture DT40 cells without native  $\text{IP}_3\text{Rs}$  and then transfected to stably express a single subtype of mammalian  $\text{IP}_3\text{R}$  (DT40- $\text{IP}_3\text{R1-3}$ ) were described previously (Tovey et al., 2006). HEK293 cells were cultured in DMEM/F-12 GlutaMAX medium with 10% FBS at 37°C in 95% air and 5%  $\text{CO}_2$ . Cells were passaged or used for experiments when they reached confluence. Plasmids were transfected into HEK cells using TransIT-LT1 reagent. The transfection efficiency of HEK cells transiently expressing CFP-TRPML1 or EGFP- $\text{IP}_3\text{R1}$  was  $\sim$ 60%, assessed by CFP or EGFP fluorescence. For double transfections (CFP-TRPML1 and EGFP- $\text{IP}_3\text{R1}$ ), the transfection efficiency was  $\sim$ 15%. To generate HEK cells expressing only  $\text{IP}_3\text{R1}$  (HEK- $\text{IP}_3\text{R1}$  cells), HEK-3KO cells were transfected with the gene encoding rat  $\text{IP}_3\text{R1}$  (lacking the S1 splice site) (Rossi et al., 2009) cloned into pcDNA3.1(-)/Myc-His B plasmid (Dohle et al., 2019). To produce HEK cells stably expressing G-CEPIA1er (HEK-G-CEPIA1er cells), wild-type HEK cells were transfected with G-CEPIA1er plasmid (Suzuki et al., 2014). To generate stable cell lines (HEK- $\text{IP}_3\text{R1}$  and HEK-G-CEPIA1er cells), cells were passaged 48 hr after transfection in medium with G418 (1 mg/mL). Selection was maintained for 2 weeks with medium changes every 3 days. Monoclonal HEK- $\text{IP}_3\text{R1}$  cell lines were selected by plating cells ( $\sim$ 1 cell/well) into 96-well plates in medium containing G418 (1 mg/mL). After 4 days, wells with only one cell were identified, cells were then grown to confluence, and cell lines were expanded and their expression of  $\text{IP}_3\text{R1}$  was confirmed by western blot using an antibody specific for  $\text{IP}_3\text{R1}$  (Rossi et al., 2009). To obtain polyclonal HEK-G-CEPIA1er cells, cells with the highest G-CEPIA1er expression ( $\sim$ 1%) were isolated using fluorescence-activated cell sorting (FACS). siRNA transfections of wild-type HEK cells used a Neon transfection system with a final siRNA concentration of 150 nM. Cells were incubated for 48 hr before use. The siRNAs used are listed in the Key Resources table.

### $\text{Ca}^{2+}$ release by $\text{IP}_3\text{Rs}$

Incubation of cells with the acetoxymethylester (AM) of Mag-fluo 4 traps low-affinity forms of the indicator ( $K_d^{\text{Ca}} = 1.15$  mM measured *in situ*) within the ER. Fluorescence, which is approximately linearly related to ER free  $[\text{Ca}^{2+}]$  (since  $[\text{Ca}^{2+}]_{\text{ER}} < K_d^{\text{Ca}}$ ), can then be used, without further calibration, to reliably report free  $[\text{Ca}^{2+}]$  within the ER lumen (Rossi and Taylor, 2020). The ER of DT40 or HEK293 cells was loaded with indicator by incubating cells with Mag-fluo 4 AM (20  $\mu\text{M}$ , 60 min, 22°C) in HEPES-buffered saline (HBS: 135 mM NaCl, 5.9 mM KCl, 11.6 mM HEPES, 1.5 mM  $\text{CaCl}_2$ , 11.5 mM glucose, 1.2 mM  $\text{MgCl}_2$ , pH 7.3) as described (Rossi et al., 2009). After washing and permeabilization with saponin (10  $\mu\text{g/mL}$ , 37°C, 2–3 min) in  $\text{Ca}^{2+}$ -free cytosol-like medium ( $\text{Ca}^{2+}$ -free CLM), cells were centrifuged (650  $\times g$ , 2 min) and resuspended in  $\text{Mg}^{2+}$ -free CLM supplemented with  $\text{CaCl}_2$  to give a final free  $[\text{Ca}^{2+}]$  of 220 nM after addition of 1.5 mM MgATP.  $\text{Ca}^{2+}$ -free CLM comprised: 20 mM NaCl, 140 mM KCl, 1 mM EGTA, 20 mM PIPES, 2 mM  $\text{MgCl}_2$ , pH 7.0. Cells ( $4 \times 10^5$  cells/well) were attached to poly-L-lysine-coated 96-well black-walled plates (Greiner Bio-One, Stonehouse, UK), and fluorescence (excitation and emission at 485 nm and 520 nm, respectively) was recorded at intervals of 1.44 s using a FlexStation III plate-reader (Molecular Devices, Sunnyvale, CA, USA). MgATP (1.5 mM) was added to initiate  $\text{Ca}^{2+}$  uptake, and when the ER had loaded to steady state with  $\text{Ca}^{2+}$  ( $\sim$ 150 s), ligands were added. Responses to the ligands show ER  $\text{Ca}^{2+}$  contents as either time courses or, in summary results, as the  $\text{Ca}^{2+}$  content recorded 20 s after addition of the stimulus. The distribution of samples across 96-well plates was varied between experiments to avoid any systematic ‘position-related’ artifacts. HEK-G-CEPIA1er cells were permeabilized and assayed as described for Mag-fluo 4-loaded cells.



## Fluorescence microscopy

Fluorescence microscopy imaging was performed using an inverted Olympus IX83 microscope equipped with either a 60 × oil-immersion objective (numerical aperture, NA 1.45) or a 100 × oil-immersion total internal reflection fluorescence (TIRF) objective (NA 1.49), a multi-line laser bank (excitation light 425 nm and 488 nm) and an iLas2 targeted laser illumination system (Cairn, Faversham, Kent, UK). Excitation light was transmitted through either a quad dichroic beam splitter (TRF89902-QUAD) or a dichroic mirror (for 425 nm; ZT442rdc-UF2) (Chroma). Emitted light was passed through appropriate filters (Cairn Optospin; peak/bandwidth: 480/40 and 525/50) and detected using an iXon Ultra 897 electron-multiplied charge-coupled device (EMCCD) camera (512 × 512 pixels, Andor). Spinning-disc confocal microscopy used a spinning disc with a 70-μm pinhole (X-Light, Crest Optics). TIRFM used the iLas2 illumination system and the penetration depth was 90–140 nm. For analyses of the distribution of CFP-TRPML1 and EGFP-IP<sub>3</sub>R1 (Figure S5F), we confirmed that there was no bleed-through between channels. Image capture and processing used MetaMorph (Molecular Devices) and Fiji (Schindelin et al., 2012). All images were corrected for background (MetaMorph) by subtracting fluorescence detected from a region without cells.

## Single-cell analyses of Ca<sup>2+</sup> release

HEK-G-CEPIA1er cells were permeabilized with saponin, and resuspended in Mg<sup>2+</sup>-free CLM supplemented with CaCl<sub>2</sub> to give a final free [Ca<sup>2+</sup>] of 220 nM after addition of 1.5 mM MgATP. Cells were attached (4 × 10<sup>5</sup> cells/well) to a poly-L-lysine-coated 8-well glass bottomed μ-slide. MgATP (1.5 mM) was added to initiate Ca<sup>2+</sup> uptake, and when the ER had loaded to steady state with Ca<sup>2+</sup> (~700 s), ligands were added.

Cells were imaged (2 s/frame) using spinning-disc confocal microscopy with a 60 × oil-immersion objective. Images were collected using MetaMorph, corrected for background fluorescence and analyzed using the Time Series Analyzer plugin (Fiji). Fluorescence intensity values from regions of interest (ROI) that delineated individual cells or ROI within individual cells are reported in arbitrary fluorescence units.

## [<sup>3</sup>H]IP<sub>3</sub> binding

IP<sub>3</sub>R1, which accounts for ~99% of IP<sub>3</sub>Rs in cerebellum (Wojcikiewicz, 1995), was purified from cerebella of adult Wistar rats using heparin-affinity chromatography (Rossi et al., 2009). The purified protein (10 μg/mL) was stored at –80°C in 500 mM NaCl, 50 mM Tris, 10% glycerol, 1 mM 2-mercaptoethanol, 1 mM benzamidine, 1 mM EGTA, 50 mM Tris, 1% CHAPS, pH 8.0. N-terminal fragments of IP<sub>3</sub>R1 (IBC, residues 224–604; NT, residues 1–604) were expressed as N-terminally tagged His<sub>6</sub>-fusion proteins in *E. coli* and cleaved from the tag with thrombin (Rossi et al., 2009). Most equilibrium-competition binding assays (4°C, 5 min) were performed in Tris-EDTA medium (TEM, 500 μL) comprising 50 mM Tris, 1 mM EDTA, pH 8.3 with [<sup>3</sup>H]IP<sub>3</sub> (21 Ci/mmol, 0.3–1.5 nM), bacterial lysate (7 μg protein) or purified IP<sub>3</sub>R1 (2 μg protein), and competing ligands (Rossi et al., 2009). Bound and free ligand were separated by centrifugation (4°C, 5 min, 14,000 × g). Non-specific binding, determined by addition of 10 μM IP<sub>3</sub>, was less than 10% of total binding.

For analyses of [<sup>3</sup>H]IP<sub>3</sub> binding under conditions that mimicked those used for functional assays (Figure 2G), equilibrium-competition binding assays (22°C, 5–10 min) were performed in Mg<sup>2+</sup>-free CLM supplemented with CaCl<sub>2</sub> to give a final free [Ca<sup>2+</sup>] of 220 nM, [<sup>3</sup>H]IP<sub>3</sub> (19.3 Ci/mmol, 7.5 nM), membranes from cerebella of adult Wistar rats (~100 μg protein) and competing ligands. Bound and free ligand were separated by centrifugation (22°C, 5 min, 14,000 × g). Non-specific binding, determined by addition of 100 μM IP<sub>3</sub>, was less than 10% of total binding.

## Nuclear patch-clamp recording from IP<sub>3</sub>Rs

The methods used for patch-clamp recording from patches excised from the outer nuclear envelope of DT40-IP<sub>3</sub>R1 cells, with K<sup>+</sup> as charge-carrier and using QuB (Qin, 2004) for analysis of currents, were as described previously (Taufiq-Ur-Rahman et al., 2009; Rossi et al., 2009). It typically took 30–45 s to establish a recording, and *P*<sub>o</sub> was then stable throughout recordings that typically lasted up to 8–10 mins.

## Western blotting

Cells were harvested in radio-immunoprecipitation assay (RIPA) buffer (150 mM NaCl, 1.0% NP-40 or Triton X-100, 0.5% sodium deoxycholate, 0.1% SDS, 50 mM Tris, pH 8.0) with protease inhibitor cocktail. The cell suspension was passed through a 25-gauge needle, incubated for 30 min at 4°C with rotation, sonicated (3 × 10 s pulses on ice), and then cleared by centrifugation (14,000 × g, 60 min, 4°C). Proteins were separated using 3%–8% or 4%–12% SDS-PAGE gels (NuPAGE), and transferred to PVDF membranes using an iBlot system. Antibodies are listed in the Key Resources table. Proteins were visualized using ECL Prime/Select western blotting detection reagents and the GeneGnome imaging system (SynGene, Cambridge, UK) and chemiluminescence was quantified using Fiji (Schindelin et al., 2012). For all quantitative analyses, we used bands for which we confirmed, by serial dilution of samples, a linear relationship between protein loading and band intensity.

## QUANTIFICATION AND STATISTICAL ANALYSES

### Simulations

Simulations first consider the number of open IP<sub>3</sub>Rs after sequential additions of IP<sub>3</sub>. The scheme assumes that IP<sub>3</sub>Rs to which four IP<sub>3</sub> molecules have bound move between three stable states, closed (C<sub>4</sub>), open (O<sub>4</sub>) and inactivated (I<sub>4</sub>), each with similar affinity for IP<sub>3</sub>.

(Figure 7E). Transitions between receptors states are described by a triangular kinetic scheme (Tveito and Lines, 2010), with  $k_1 = 0.4 \text{ s}^{-1}$ ,  $k_2 = 0.2 \text{ s}^{-1}$  and  $k_3 = 0.004 \text{ s}^{-1}$ , but the scheme includes an irreversible step in a way that is reminiscent of a published model for adaptation in cell signaling (Ferrell, 2016). The transitions between these states (rate constants,  $k_i$ ,  $0.004 - 0.4 \text{ s}^{-1}$ , and 100-times slower for  $k_{-i}$ ) are much slower than the rates of IP<sub>3</sub> association ( $\sim 3.5 \times 10^7 \text{ M}^{-1} \cdot \text{s}^{-1}$ ;  $k_{\text{on}} \sim 3.5 \text{ s}^{-1}$  with 100 nM IP<sub>3</sub>) (Hannaert-Merah et al., 1994) or dissociation ( $\sim 28 \text{ s}^{-1}$ , estimated from the  $K_D$  in Figure 2G). Our scheme therefore assumes that for each IP<sub>3</sub> concentration, there is a fixed number of IP<sub>3</sub>Rs with all four IP<sub>3</sub>-binding sites occupied, determined by the  $K_D^{\text{IP}_3}$  (794 nM) and the number of IP<sub>3</sub>Rs/cell (49,146 in HEK-IP<sub>3</sub>R1 cells) (Figure 7B). IP<sub>3</sub> addition is simulated by an immediate increase in  $C_4$ . Simulations are performed stochastically, with each IP<sub>3</sub>R simulated independently. The probability of transition  $i$  is equal to  $k_i \cdot \Delta t$ . At each time step (12.5 ms), the algorithm generates a number  $X$  drawn uniformly at random on the  $[0, 1]$  interval. If  $X < k_i \cdot \Delta t$ , the IP<sub>3</sub>R changes state; otherwise it remains in the same state. The behavior of the IP<sub>3</sub>R population is obtained by summing the number of IP<sub>3</sub>Rs in each state at every time step. The output provides the temporal evolution of the number of open IP<sub>3</sub>Rs. The same scheme and parameters were used to simulate the behavior of IP<sub>3</sub>Rs within a single wild-type HEK cell, for which we determined the expression level to be  $9101 \pm 934$  IP<sub>3</sub>Rs/cell.

To simulate the change in ER free  $[\text{Ca}^{2+}]$  ( $C_{\text{ER}}$ ) over time, we consider the following equation:

$$\frac{dC_{\text{ER}}}{dt} = -(k_{\text{leak}} + k_{\text{rel}} \cdot O_4) \cdot (C_{\text{ER}} - C) \quad (1)$$

where  $O_4$  is the number of open IP<sub>3</sub>Rs determined from the stochastic simulations,  $k_{\text{leak}}$  is the rate constant for the IP<sub>3</sub>-independent  $\text{Ca}^{2+}$  leak from the ER ( $1.8 \times 10^{-4} \text{ s}^{-1}$ , see Analysis section),  $k_{\text{rel}}$  is the rate constant for  $\text{Ca}^{2+}$  flux through an open IP<sub>3</sub>R ( $0.0008 \text{ s}^{-1}$ ). We estimated  $k_{\text{rel}}$  by assuming that the free  $[\text{Ca}^{2+}]$  within the ER was 500  $\mu\text{M}$ , the buffer capacity was 5 (hence, total ER  $[\text{Ca}^{2+}] = 2.5 \text{ mM}$ ; see Analysis section), and an open IP<sub>3</sub>R conducts  $5 \times 10^5 \text{ Ca}^{2+} \text{ s}^{-1}$  (Vais et al., 2010).  $C$ , the cytosolic free  $[\text{Ca}^{2+}]$ , is fixed at 220 nM by the EGTA included in CLM. At the beginning of each simulation,  $C_{\text{ER}}$  is set to 500  $\mu\text{M}$  (see Rossi and Taylor, 2020) and then computed at each time step for the corresponding  $O_4$ . The fraction of releasable ER  $\text{Ca}^{2+}$  was set to 80%.

To simulate experiments where the ER can refill through SERCA, we used:

$$\frac{dC_{\text{ER}}}{dt} = -(k_{\text{leak}} + k_{\text{rel}} \cdot O_4) \cdot (C_{\text{ER}} - C) + (500 - C_{\text{ER}}) / \tau_{\text{SERCA}} \quad (2)$$

with  $\tau_{\text{SERCA}} = 100 \text{ s}$ .

Codes for the simulations are available from <https://github.com/genedupont/Quantal>.

## Analysis

Rates of  $\text{Ca}^{2+}$  release evoked by IP<sub>3</sub>, ionomycin, carbachol or **2**, corrected for the basal  $\text{Ca}^{2+}$  leak ( $J_{\text{leak}}$ ), were calculated by fitting a mono-exponential function to the ER  $\text{Ca}^{2+}$  content determined from the time of adding CPA alone. The derivative of this relationship at each time provides  $J_{\text{leak}}$ . From the relationship between  $J_{\text{leak}}$  and ER  $\text{Ca}^{2+}$  content (fitted to a second-degree polynomial or exponential function),  $J_{\text{leak}}$  was estimated at each time and subtracted from the observed  $\text{Ca}^{2+}$  release to identify the  $\text{Ca}^{2+}$  release evoked by IP<sub>3</sub>, ionomycin, carbachol or **2** (Figures 1F, 1L, 3B, S3D, and S4B).

For each IP<sub>3</sub> or ionomycin concentration, the time evolution of ER free  $[\text{Ca}^{2+}]$  ( $[\text{Ca}^{2+}]_{\text{ER}}$ ) was then numerically reconstructed by integration over time of the IP<sub>3</sub>- or ionomycin-evoked  $\text{Ca}^{2+}$  flux.  $J_{\text{leak}}$  values from  $[\text{Ca}^{2+}]_{\text{ER}}$  of 500  $\mu\text{M}$  were also used to estimate the rate constant of  $\text{Ca}^{2+}$  leak from the ER ( $k_{\text{leak}} = 1.8 \times 10^{-4} \text{ s}^{-1}$ ) used in the simulations. To obtain the evolution of open receptors (Figures 7R–7T), the leak-independent  $\text{Ca}^{2+}$  flux was subtracted from the rate of  $\text{Ca}^{2+}$  release before division of each instantaneous rate by the corresponding  $\text{Ca}^{2+}$  gradient. Following Equation (1), this gives the time-evolution of the number of open receptors in arbitrary units.

To estimate the total ER  $\text{Ca}^{2+}$  content of a single HEK cell, we assume a luminal free  $[\text{Ca}^{2+}]$  of  $\sim 500 \mu\text{M}$  (Rossi and Taylor, 2020), a buffer ratio of  $\sim 5$  (Prins and Michalak, 2011) (suggesting a total luminal  $[\text{Ca}^{2+}]$  of  $\sim 2.5 \text{ mM}$ ); a cell volume of  $1.1 \times 10^{12} \text{ L}$  (<http://bionumbers.hms.harvard.edu/search.aspx>) of which  $\sim 10\%$  is occupied by the nucleus and  $\sim 35\%$  of the remaining cytoplasm is occupied by ER ( $\sim 3.64 \times 10^{-13} \text{ L}$ ) (Valm et al., 2017). Hence, we estimate the total ER  $\text{Ca}^{2+}$  content within a single HEK cell to be  $\sim 9 \times 10^{-16} \text{ mol}$ .

For equilibrium binding and concentration-effect relationships, results from each experiment were fitted to Hill equations (PRISM) from which  $\text{pIC}_{50}$  (-log of half-maximal inhibitory concentration) or  $\text{pEC}_{50}$  (-log of half-maximally effective concentration) values were determined.  $K_D^{\text{ligand}}$  was calculated from:  $K_D^{\text{ligand}} = \text{IC}_{50}^{\text{ligand}} - [^3\text{H-IP}_3] / K_D^{\text{IP}_3}$ . In functional assays, dose ratios (DR) were used to calculate antagonist affinities (Arunlakshana and Schild, 1959):  $K_D^{\text{antagonist}} = [\text{antagonist}] / (\text{DR} - 1)$ . Statistical analyses of IP<sub>3</sub> sensitivity used  $\text{pEC}_{50}$  and  $\text{pK}_D$  values.

## Statistical analyses

Experiments were performed without prior power calculations, blinding or systematic randomization. The distribution of treatments across wells in multi-well plates was varied between experiments to avoid any systematic bias arising from place-related effects. Statistical significance was assessed using Student's  $t$  test or one-way repeated ANOVA followed by Bonferroni's multiple comparisons test, with  $*p < 0.05$  considered significant (PRISM). The numbers of independent experiments and replicates for each biological experiment are indicated in figure legends. Details of all statistical tests and exact  $p$  values are provided in Supplemental materials and methods.